


Targeting PD-L2–RGMb overcomes microbiome-related immunotherapy resistance

<https://doi.org/10.1038/s41586-023-06026-3>

Received: 4 February 2022

Accepted: 28 March 2023

Published online: 3 May 2023

 Check for updates

Joon Seok Park^{1,9}, Francesca S. Gazzaniga^{1,2,3,9}, Meng Wu¹, Amalia K. Luthens¹, Jacob Gillis¹, Wen Zheng¹, Martin W. LaFleur¹, Sarah B. Johnson⁴, Golnaz Morad⁴, Elizabeth M. Park^{4,5,6}, Yifan Zhou^{4,5}, Stephanie S. Watowich^{4,5}, Jennifer A. Wargo^{4,6,7}, Gordon J. Freeman^{8,10}✉, Dennis L. Kasper^{1,10}✉ & Arlene H. Sharpe^{1,3,10}✉

The gut microbiota is a crucial regulator of anti-tumour immunity during immune checkpoint inhibitor therapy. Several bacteria that promote an anti-tumour response to immune checkpoint inhibitors have been identified in mice^{1–6}. Moreover, transplantation of faecal specimens from responders can improve the efficacy of anti-PD-1 therapy in patients with melanoma^{7,8}. However, the increased efficacy from faecal transplants is variable and how gut bacteria promote anti-tumour immunity remains unclear. Here we show that the gut microbiome downregulates PD-L2 expression and its binding partner repulsive guidance molecule b (RGMb) to promote anti-tumour immunity and identify bacterial species that mediate this effect. PD-L1 and PD-L2 share PD-1 as a binding partner, but PD-L2 can also bind RGMb. We demonstrate that blockade of PD-L2–RGMb interactions can overcome microbiome-dependent resistance to PD-1 pathway inhibitors. Antibody-mediated blockade of the PD-L2–RGMb pathway or conditional deletion of RGMb in T cells combined with an anti-PD-1 or anti-PD-L1 antibody promotes anti-tumour responses in multiple mouse tumour models that do not respond to anti-PD-1 or anti-PD-L1 alone (germ-free mice, antibiotic-treated mice and even mice colonized with stool samples from a patient who did not respond to treatment). These studies identify downregulation of the PD-L2–RGMb pathway as a specific mechanism by which the gut microbiota can promote responses to PD-1 checkpoint blockade. The results also define a potentially effective immunological strategy for treating patients who do not respond to PD-1 cancer immunotherapy.

Antibodies that block programmed death 1 (PD-1) or programmed death ligand 1 (PD-L1) have been approved for more than 25 different tumours. However, the response rates for PD-1–PD-L1 blockade in approved indications range from 13% to 69% depending on the tumour type^{9,10}. There is substantial interest in understanding the factors that regulate the responsiveness to PD-1 inhibitors to develop strategies to benefit more patients. Studies have shown that the gut microbiota can modulate the efficacy of PD-1 pathway inhibitors in cancer^{7,8}. These findings have stimulated the investigation of probiotic bacteria and faecal transplants to promote anti-tumour responses to PD-1 immunotherapy. However, inconsistent results highlight the need to understand mechanisms by which the gut microbiota can promote anti-tumour immunity. Our goal was to identify targetable immunological mechanisms by

which the gut microbiome regulates anti-tumour effects of cancer immunotherapy.

The gut microbiota enhances immunotherapy

We established mouse tumour models in which the anti-tumour response depended on gut bacteria (Fig. 1a). When MC38 colon carcinoma cells were subcutaneously implanted, conventional specific pathogen-free (SPF) mice containing the gut microbiome of mice from the vendor (Taconic) responded to anti-PD-L1 therapy (Extended Data Fig. 1a). By contrast, germ-free (GF) mice did not respond to anti-PD-L1 or anti-PD-1 treatment (Extended Data Fig. 1b,c). Reconstitution of GF mice with healthy human microbiota (HMB) (Fig. 1b) or healthy

¹Department of Immunology, Blavatnik Institute, Harvard Medical School, Boston, MA, USA. ²Molecular Pathology Unit, Massachusetts General Hospital, Charlestown, MA, USA. ³Department of Pathology, Harvard Medical School, Boston, MA, USA. ⁴Program for Innovative Microbiome and Translational Research, Department of Genomic Medicine, The University of Texas MD Anderson Cancer Center, Houston, TX, USA. ⁵Department of Immunology, The University of Texas MD Anderson Cancer Center, Houston, TX, USA. ⁶Department of Surgical Oncology, The University of Texas MD Anderson Cancer Center, Houston, TX, USA. ⁷Department of Genomic Medicine, The University of Texas MD Anderson Cancer Center, Houston, TX, USA. ⁸Department of Medical Oncology, Dana-Farber Cancer Institute, Harvard Medical School, Boston, MA, USA. ⁹These authors contributed equally: Joon Seok Park, Francesca S. Gazzaniga. ¹⁰These authors jointly supervised this work: Gordon J. Freeman, Dennis L. Kasper, Arlene H. Sharpe. ✉e-mail: gordon_freeman@dfci.harvard.edu; dennis_kasper@hms.harvard.edu; arlene_sharpe@hms.harvard.edu

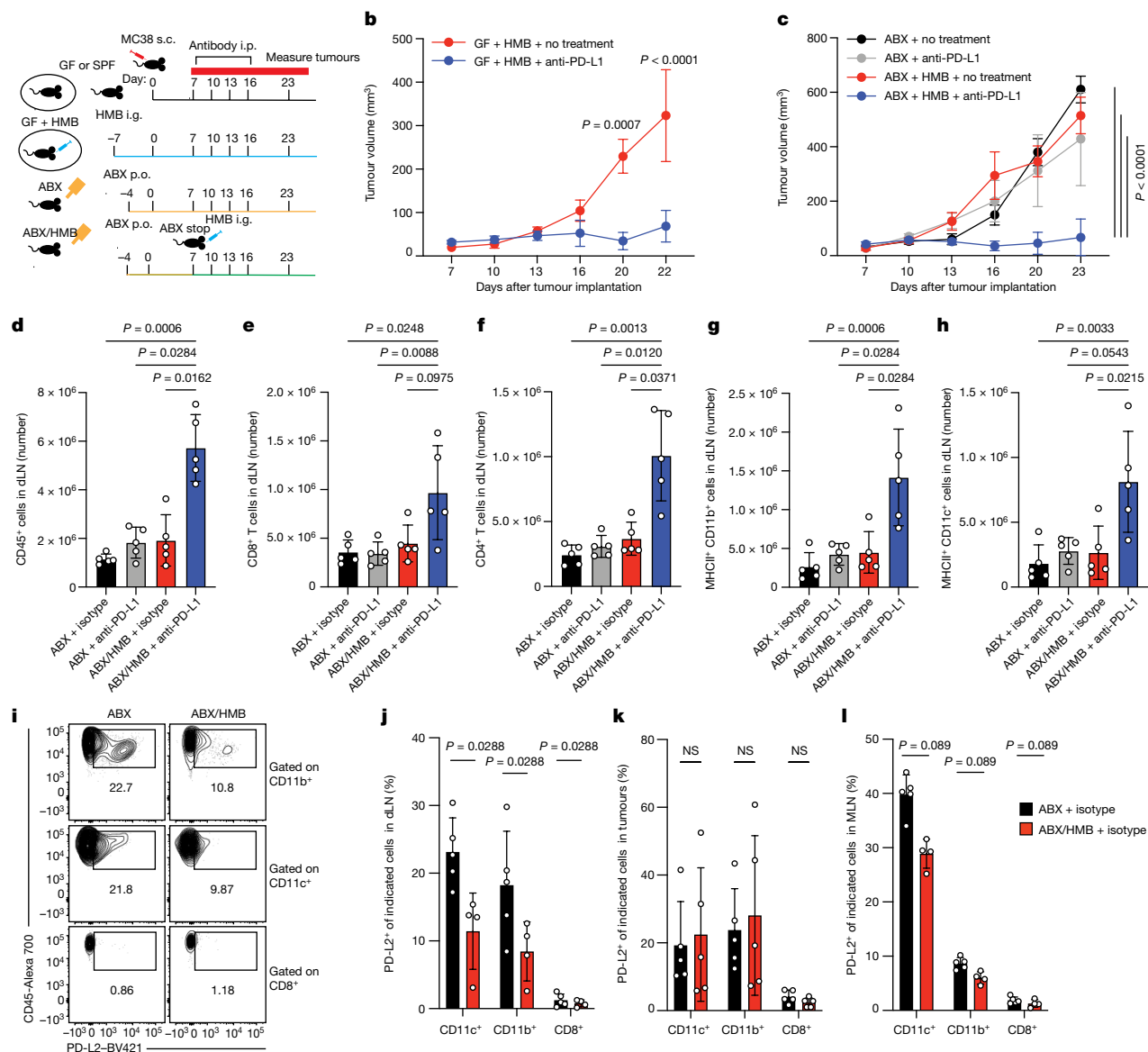


Fig. 1 | The microbiota promotes an effective anti-tumour response to PD-L1 blockade and suppresses PD-L2 expression. **a**, Schematic of the experimental design. ABX, antibiotic; i.g., intragastric (oral gavage); i.p., intraperitoneally; p.o., orally; s.c., subcutaneously. **b**, MC38 tumour growth with or without anti-PD-L1 treatment in GF mice given HMB. $n = 10$ mice per group, representative experiment of 4 individual experiments. Significance, shown on graph, calculated using two-way analysis of variance (ANOVA) and Sidak's multiple comparisons test. **c**, Same as **b** but in ABX-treated and ABX/HMB-treated mice. $n = 4$ mice for ABX groups, $n = 5$ mice for ABX/HMB groups, representative experiment of 5 individual experiments. Significance at day 23 is shown and was calculated using two-way ANOVA with Tukey's multiple comparisons test. For **b** and **c**, error bars show the mean and s.e.m. **d–h**, ABX-treated mice and ABX/HMB-treated mice were treated as in **a** and

killed on day 13 after tumour implantation. Numbers of CD45⁺ cells (**d**), CD8⁺ T cells (**e**), CD4⁺ T cells (**f**), MHCII⁺CD11b⁺ cells (**g**) and MHCII⁺CD11c⁺ cells (**h**) in tumour dLNs. For **d–h**, $n = 5$ mice per group, representative experiment of 2 individual experiments. P values are indicated on the graphs and calculated using one-way ANOVA with Dunn's multiple comparisons test, and error bars show the mean and s.d. **i**, Contour plots of representative examples of PD-L2 expression gating in dLNs. **j–l**, Percent of PD-L2 expression on MHCII⁺CD11c⁺ cells, MHCII⁺CD11b⁺ cells and CD8⁺ T cells in dLNs (**j**; $n = 5$ mice for ABX, $n = 4$ mice for ABX/HMB), tumours (**k**; $n = 5$ mice per group) and MLNs (**l**; $n = 5$ mice for ABX, $n = 4$ mice for ABX/HMB). For **j–l**, significance determined using unpaired, two-tailed Mann–Whitney test and significant P values are indicated on the graphs. NS, not significant. Error bars show s.d., and data are representative experiment of two different experiments.

mouse microbiota (MMB)¹¹ (Extended Data Fig. 1d) promoted a strong anti-tumour response to anti-PD-L1 therapy. To further investigate the immunoregulatory influence of human bacteria, we used HMB as our responder microbiota. Similar to GF mice (Extended Data Fig. 1b,c), depletion of gut commensals with a cocktail of four oral antibiotics (Fig. 1c and Extended Data Fig. 1e) prevented anti-PD-L1-mediated or anti-PD-1-mediated suppression of MC38 tumour growth. By contrast, mice given antibiotics until day 7 after tumour implantation and then orally gavaged with HMB (termed ABX/HMB treatment) reduced MC38 tumour growth in response to anti-PD-L1 or anti-PD-1 treatment

(refs. 11,12) (Fig. 1c and Extended Fig. 1e). A comparison of tumours at day 24 in antibody-treated mice and ABX/HMB-treated mice, both administered an anti-PD-L1 antibody, revealed that the mice treated with ABX/HMB and anti-PD-L1 had a significant increase in the CD8⁺ to regulatory T (T_{reg}) cell ratio. In detail, they exhibited an increased frequency of CXCR5⁺TIM-3⁺CD8⁺ progenitor T cells, a decreased frequency of the terminally exhausted PD-1⁺TIM-3⁺CD8⁺ T cells and enhanced CD8⁺ T cell effector functions, including increased frequencies of granzyme B⁺CD8⁺ T cells, TNF⁺CD8⁺ T cells, IFN γ ⁺CD8⁺ T cells, TNF⁺IFN γ ⁺CD8⁺ T cells and IFN γ ⁺CD4⁺ T cells. These results indicate

that HMB promotes CD8⁺ and CD4⁺ T cell function in the responding tumours (Extended Data Fig. 2a–h). The enhanced response of ABX/HMB-treated mice compared with mice treated with antibiotics alone to anti-PD-L1 or anti-PD-1 enabled the examination of mechanisms by which the gut microbiota regulates anti-tumour responses during anti-PD-L1 or anti-PD-1 treatment (Fig. 1c and Extended Data Fig. 1e).

Gut microbiotas affect PD-L2 expression

Because gut microbiotas affect the efficacy of PD-1–PD-L1 blockade, we proposed that gut bacteria can modulate the expression of checkpoint molecules and thereby affect anti-tumour immune responses. Therefore, we compared the expression of several immune checkpoint molecules on immune cells from tumours, from tumour draining lymph nodes (dLNs) and from mesenteric lymph nodes (MLNs) in antibiotic-treated mice and ABX/HMB-treated mice. To distinguish between checkpoint molecules that have a causative role in anti-tumour responses rather than are a consequence of the response, we analysed immune cells at days 10–13 after tumour implantation, before tumour sizes diverge (Fig. 1c). Frequencies of PD-1⁺, PD-1⁺TIM-3⁺, CD44⁺PD-1⁺ or IFN γ ⁺ CD8⁺ T cells, which have previously been shown to increase at later time points in the microbiota-mediated response to PD-1 blockade^{3,4}, did not significantly differ at the day 13 time point in tumours of antibiotic-treated mice administered an anti-PD-L1 antibody (Extended Data Fig. 2i–l). This was in contrast to ABX/HMB-treated mice given an anti-PD-L1 antibody and analyzed at day 24, which indicates that this time point was before PD-1 blockade significantly enhanced CD8⁺ T cell anti-tumour function in these responder mice. However, at day 13 after tumour implantation, the numbers of CD45⁺ immune cells, CD8⁺ T cells, CD4⁺ T cells and MHCII⁺CD11b⁺ cells, but not MHCII⁺CD11c⁺ cells, in the dLNs were coordinately increased in ABX/HMB-treated mice given an anti-PD-L1 antibody compared with mice given antibiotics only or isotype control (Fig. 1d–h). Differences in expression of immune checkpoint molecules in dendritic cells (DCs) and myeloid cells but not T cells were also observed. Moreover, PD-L2 expression was significantly decreased, whereas PD-L1 expression was increased on CD11b⁺MHCII⁺ and CD11c⁺MHCII⁺ cells in the dLNs of ABX/HMB-treated mice compared with antibiotic-treated mice. CD80, CD86 and ICOSL did not show significant differences in expression levels (Fig. 1i, j and Extended Data Fig. 2m–p). Thus, PD-L2 expression is downregulated whereas PD-L1 is increased on these populations in dLNs of responder mice (ABX/HMB plus anti-PD-L1). These data suggest that the gut microbiota regulates signalling pathways involved in the expression of co-inhibitory molecules.

The reduced level of PD-L2 expression in responder mice led us to propose that high expression of this co-inhibitory molecule in non-responder mice inhibits anti-tumour immunity. Compared with antibiotic-treated mice, PD-L2 expression was reduced at both day 10 and day 13 on CD11c⁺ and CD11b⁺ cells in the dLNs and MLNs but not in tumours in ABX/HMB-treated mice (Fig. 1i–l and Extended Data Fig. 2q). PD-L2 was similarly reduced at day 10 in dLNs of SPF mice compared with GF mice (Extended Data Fig. 2r). PD-L2 expression was still reduced at day 24 after tumour implantation on CD11c⁺ cells in the dLNs and MLNs but not in tumours or spleens of ABX/HMB-treated mice (Extended Data Fig. 2s–v). This result suggests that HMB colonization results in reduced PD-L2 expression on CD11c⁺ DCs in the gut and tumour dLNs, but does not cause universally reduced PD-L2 expression. Anti-tumour effects of PD-1 pathway blockade derive, at least in part, from T cell responses in the dLN¹³, and there was reduced PD-L2 expression in dLNs of the responder HMB mice. Therefore, we proposed that high PD-L2 expression on antigen-presenting cells in dLNs of non-responder antibiotic-treated mice is important for inhibiting anti-tumour immunity. Because the anti-PD-1 treatment was not effective in GF mice or in antibiotic-treated mice, even though it blocks interactions with both PD-L1 and PD-L2, we considered whether PD-L2 is working through a receptor other than PD-1.

Combined therapy in GF, antibiotic-treated and SPF mice

To directly investigate the contribution of upregulated PD-L2 expression to impaired anti-tumour responses in GF mice and antibiotic-treated mice that do not respond to PD-L1 or PD-1 blockade alone, we treated GF mice and antibiotic-treated mice with a combination of anti-PD-L2 and anti-PD-L1 monoclonal antibodies. Combined anti-PD-L1 and anti-PD-L2 (3.2 clone) antibody treatment reduced MC38 tumour growth in GF mice and antibiotic-treated mice. By contrast, treatment with either antibody alone failed to inhibit tumour growth (Fig. 2a, b). Combined anti-PD-L2 antibody with anti-PD-1 or anti-PD-L1 antibody treatment also reduced the growth of MB49 bladder tumours in antibiotic-treated mice (Extended Data Fig. 3a, b). Moreover, combined anti-PD-L2 and anti-PD-L1 treatment reduced the growth of B16 melanoma tumours expressing ovalbumin (B16-OVA) and the growth of Py8119 mammary tumours expressing ovalbumin (Py8119-OVA) in SPF mice, significantly more than treatment with either antibody alone (Extended Data Fig. 3c, d). These results indicate that this combination therapy can improve responses in the context of an endogenous microbiota. Anti-PD-L1 and anti-PD-L2 combination therapy promoted an anti-tumour response in SPF mice with MC38 tumours, but this combination was not significantly better than anti-PD-L1 alone, which already promoted a strong response (Extended Data Fig. 3e). In SPF mice, anti-PD-L2 treatment did not enhance the efficacy of anti-PD-L1 or PD-1 in E0771 breast cancer tumours or of anti-PD-L1 in Lewis lung carcinoma cells expressing ovalbumin (LLC-OVA) (Extended Data Fig. 3f–h). Therefore, combined blockade of PD-L2 and PD-1 or PD-L1 may be beneficial for treating multiple, but not all, cancers.

Combined therapy with patient microbiota

We next tested the translational potential of anti-PD-L1 and anti-PD-L2 combination therapy in humans. We colonized groups of GF mice (in a blinded fashion) with faecal samples from the following patients: a patient with melanoma who had a complete response to anti-PD-1 therapy (CR); two patients with melanoma who did not respond to anti-PD-1 therapy (non-responders, NR1 and NR2; Extended Data Fig. 4a). 16S rRNA gene sequencing of stool samples from mice colonized with patient stool for 1 week before tumour implantation revealed significant differences in each cohort of mice colonized with stool from a different patient (Extended Data Fig. 4a–h).

Consistent with the clinical responses of the patients to anti-PD-1 therapy, mice colonized with stool from the CR patient had significantly smaller MC38 tumours when treated with anti-PD-L1 monotherapy than mice colonized with stool samples from the NR1 or NR2 patients¹⁴ (Extended Data Fig. 4i). Given that the response to anti-PD-1 is already good, combination therapy did not significantly increase the anti-tumour response compared with monotherapy in mice colonized with stool from the CR patient. Notably, combined anti-PD-L1 and anti-PD-L2 therapy significantly improved the anti-tumour response when compared with monotherapy in mice colonized with stool from the NR1 or NR2 patients and had significantly increased overall survival (Fig. 2c–e and Extended Data Fig. 4j).

A gut commensal can suppress PD-L2

Next we tested whether specific bacteria in HMB can induce PD-L2 downregulation on DCs in the dLNs and enhance anti-PD-L1-mediated anti-tumour responses. To determine which bacteria from HMB are associated with anti-PD-L1-mediated anti-tumour responses, we gavaged antibiotic-treated mice with HMB at day 7 after tumour implantation and maintained them on a single antibiotic for the duration of the experiment to select for different populations of gut bacteria. Vancomycin, which mainly targets Gram-positive bacteria, and metronidazole,

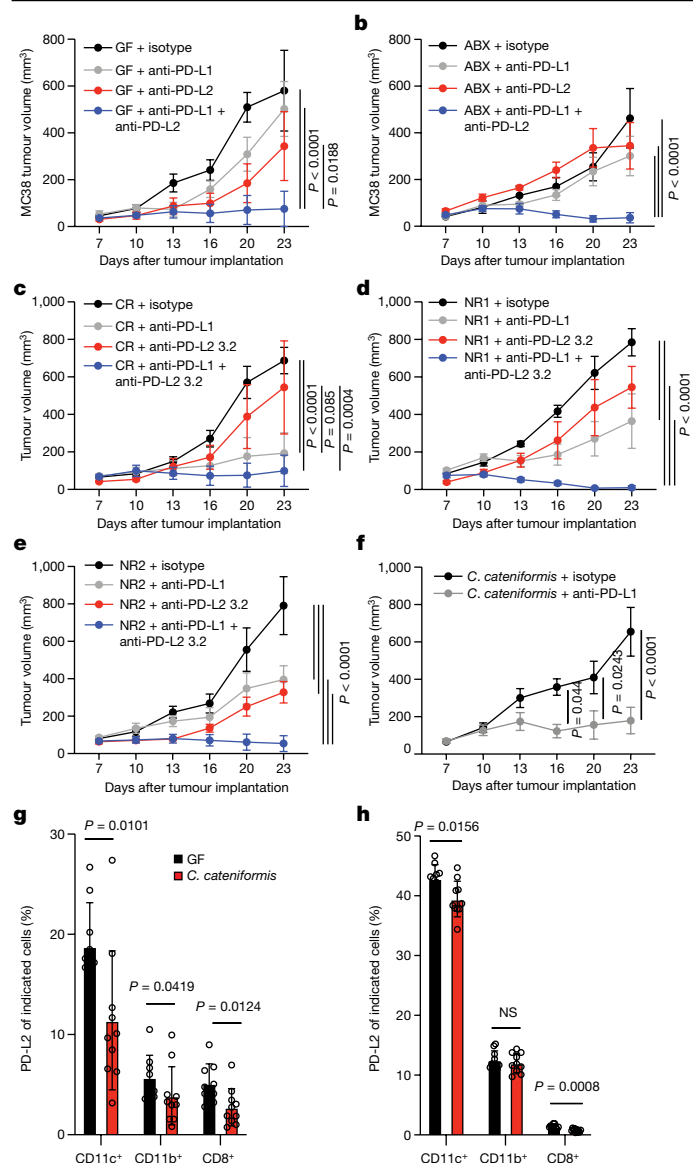


Fig. 2 | Anti-PD-L2 antibody blockade or colonization with *C. cateniformis* in combination with PD-L1 blockade promotes anti-tumour responses in non-responder GF mice or antibiotic-treated mice. a, b, MC38 tumour growth in GF mice (**a**) and ABX-treated mice (**b**). For **a** and **b**, $n = 4$ mice for isotype, $n = 5$ mice for anti-PD-L1, anti-PD-L2, and anti-PD-L1 plus anti-PD-L2. Data are representative of three experiments. **c–e**, MC38 tumour growth in GF mice colonized with stool from patients with melanoma treated with anti-PD-1 therapy. **c**, Mice were colonized with stool from a CR patient. $n = 6$ mice for isotype, anti-PD-L1, and anti-PD-L1 plus anti-PD-L2 groups, $n = 5$ mice for anti-PD-L2 group. **d**, Mice were colonized with stool from patient NR1. $n = 5$ mice for isotype, $n = 6$ mice for anti-PD-L1 and anti-PD-L1 plus anti-PD-L2, $n = 3$ for anti-PD-L2. **e**, Mice were colonized with stool from patient NR2. $n = 5$ mice for isotype, anti-PD-L1, anti-PD-L2 groups, $n = 6$ for anti-PD-L1 plus anti-PD-L2 groups. For **a–e**, significance was calculated using two-way ANOVA and Tukey's multiple comparisons test. Significant P values for day 23 are shown, and error bars show the mean and s.e.m. **f**, MC38 tumour growth in GF mice colonized with *C. cateniformis*. $n = 10$ mice per group. Significance determined using two-way ANOVA with Sidak's multiple comparisons test. Significant P values are indicated, and error bars represent the s.e.m. **g, h**, Per cent of PD-L2 expression on indicated cells from GF mice or *C. cateniformis*-colonized mice at day 10 after tumour implantation in dLNs (**g**; $n = 9$ mice for GF mice, $n = 10$ mice for *C. cateniformis*-colonized mice) and in MLNs (**h**; $n = 10$ mice per group). For **g** and **h**, significance was determined using unpaired, two-tailed, Mann–Whitney test. P values are indicated, and error bars show the mean and s.d.

which mainly targets anaerobic bacteria, were individually sufficient to abrogate anti-PD-L1 anti-tumour responses. Ampicillin, which can target some Gram-positive and some Gram-negative bacteria, dampened anti-PD-L1 anti-tumour responses, but tumour volumes did not significantly differ from mice given HMB and anti-PD-L1 treatment. Neomycin, which mainly targets aerobic and facultative Gram-negative bacteria, did not significantly change anti-PD-L1 anti-tumour responses compared with combined HMB and anti-PD-L1 treatment (Extended Data Fig. 5a–d). These data suggest that Gram-positive anaerobes in HMB are disproportionately responsible for promoting anti-PD-L1 anti-tumour responses. 16S rRNA sequencing of stool samples at days 13 and 23 after implantation revealed significant differences in microbes between groups treated with the four antibiotics (Extended Data Fig. 5e–g). By comparing stool from anti-PD-L1 responder mice (HMB colonized and neomycin treated) with stool from non-responder mice (treated with the four antibiotics or with ampicillin, vancomycin or metronidazole alone), we identified three genera from the order Clostridiales (Gram-positive anaerobes; Extended Data Fig. 5h) and two Gram-negative bacteria (family, Porphyromonadaceae, genus *Parabacteroides* and family Rikenellaceae) associated with responses to anti-PD-L1 treatment. Although the 16S rRNA sequencing results revealed that multiple genera from HMB have the potential to promote anti-tumour immunity, our antibiotic data indicated that Gram-positive anaerobes from HMB were associated with an anti-tumour response. Therefore, we focused on identifying Gram-positive anaerobes from our HMB stock, potentially from the order Clostridiales, that could promote an anti-PD-L1-mediated anti-tumour response^{15,16}. A combination of antibiotic selection, selective media and sequencing led to the identification of two species (*Coprobacillus cateniformis* and *Erysipelatoclostridium ramosum*) that could enhance anti-PD-L1-mediated anti-tumour responses when monocolonized into mice (Fig. 2f and Extended Data Fig. 6a–e). Bulk 16S rRNA gene sequencing of HMB did not provide sufficient sequence specificity to identify *C. cateniformis*. However, when primers specific to *C. cateniformis* were used¹⁷, *C. cateniformis* could be detected in HMB stock, but not in Taconic stool (Extended Data Fig. 6f). The lack of strain-specific resolution for *C. cateniformis* with 16S rRNA gene sequencing of stool could explain why few studies identify *C. cateniformis* from bulk 16S rRNA gene sequencing. Similar to other studies^{17,18}, it was only when individual colonies were isolated and the full-length 16S gene was sequenced that *C. cateniformis* was identified. Therefore, isolation of individual strains and full-length sequencing of individual colonies may be needed to fully understand which bacterial strains may be best for effective live microorganism-enhanced immunotherapy.

Colonization of GF mice with *C. cateniformis* but not *E. ramosum* significantly reduced PD-L2 expression in CD11b⁺ cells and CD11c⁺ cells in the tumour dLNs and reduced PD-L2 expression in CD11c⁺ cells in the MLNs (Fig. 2g, h and Extended Data Fig. 6g–h). Additionally, treatment of bone-marrow-derived dendritic cells (BMDCs) with soluble surface extracts of *C. cateniformis* downregulated PD-L2 expression (Fig. 3a), and this suppression depended on MYD88 (Extended Data Fig. 7a). These data demonstrate that *C. cateniformis* can downregulate PD-L2 expression on DCs in vivo and in vitro.

As observed with ABX/HMB-treated mice and antibiotic-treated mice, mice monocolonized with *C. cateniformis* had increased frequencies of dLN CD45⁺ cells compared with GF mice, with significant increases specifically in MHCII⁺CD11b⁺ cells and MHCII⁺CD11c⁺ cells 13 days after tumour implantation (Extended Data Fig. 7b–f). At day 18 after tumour implantation, mice treated with both *C. cateniformis* and an anti-PD-L1 antibody had increased percentages of tumour-infiltrating CD8⁺ T cells expressing granzyme B, IFN γ and TIM-3⁺PD-1⁺ (similar to ABX/HMB-treated mice) but not TNF (Extended Data Fig. 7g–j). This result indicates that *C. cateniformis* recapitulates many of the beneficial immunological effects of HMB, but that other bacteria in HMB have additional immunological effects.

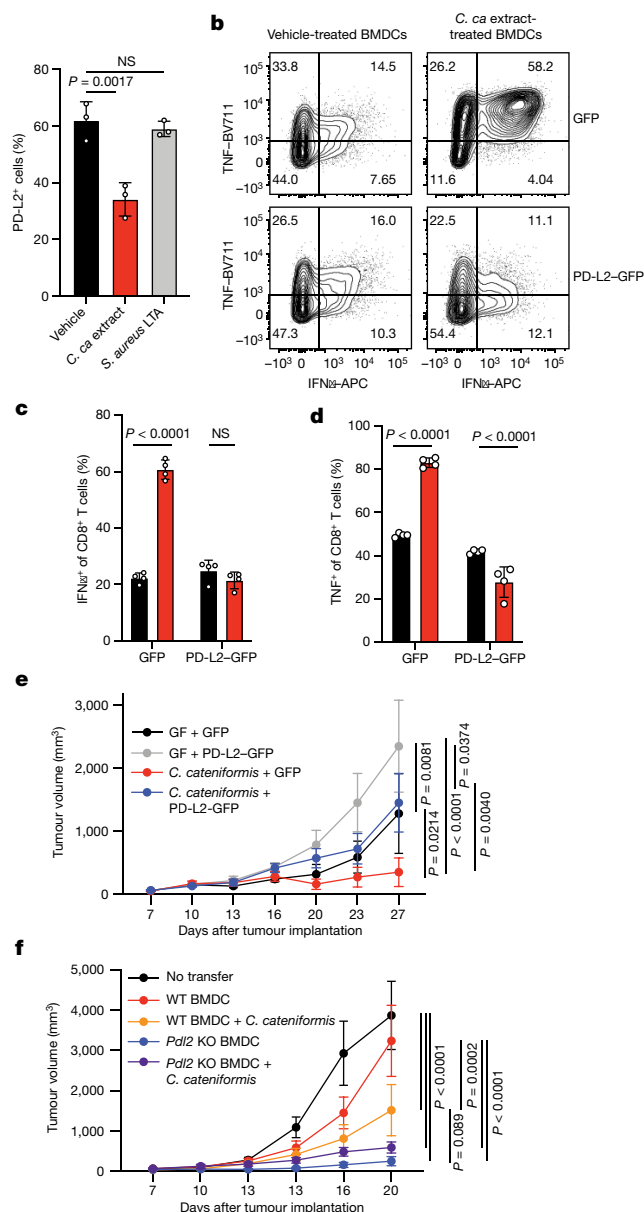


Fig. 3 | *C. cateniformis* promotes anti-tumour immunity by downregulating PD-L2. **a**, Per cent of PD-L2 expression after treatment of BMDCs with vehicle, 10 $\mu\text{g ml}^{-1}$ surface extracts from *C. cateniformis* (*C. ca* extract) or 10 $\mu\text{g ml}^{-1}$ lipoteichoic acid (LTA) from *Staphylococcus aureus* as a control for Gram-positive surface molecules. $n = 3$ wells per group, representative experiment of 2 experiments. Significance determined using one-way ANOVA with Tukey's multiple comparisons test, and error bars show the mean and s.d. **b–d**, BMDCs transduced with GFP lentivirus (GFP) or lentivirus expressing GFP and PD-L2 (PD-L2-GFP) were treated with *C. cateniformis* extract 24 h before co-culture with CD8⁺ T cells. Expression levels were measured by flow cytometry. **b**, Example of flow cytometry plots of IFN γ and TNF expression by CD8⁺ T cells. Quantification of per cent of IFN γ ⁺ (**c**) and TNF⁺ (**d**) CD8⁺ T cells. $n = 4$ wells per group. For **c** and **d**, significance was calculated using two-way ANOVA with Sidak's multiple comparisons test. Significant *P* values are indicated, and error bars show the mean and s.d. **e**, B16-OVA tumour growth in GF mice and *C. cateniformis*-monocolonized mice injected with GFP or GFP-PD-L2 (PD-L2 overexpression) BMDCs at tumour site 3 days after tumour implantation. $n = 9$ mice for GF mice plus GFP and for *C. cateniformis*-colonized mice plus GFP-PD-L2, $n = 8$ mice for GF mice plus GFP-PD-L2, $n = 10$ mice for *C. cateniformis*-colonized mice plus GFP. **f**, B16-OVA tumour growth in SPF mice injected at the tumour site with WT or *Pdl2* KO BMDCs treated with or without *C. cateniformis* extract. $n = 10$ mice per group. For **e** and **f**, significance was calculated using Tukey's multiple comparisons test. Significant *P* values are indicated, and error bars show the mean and s.e.m.

PD-L2 suppression on DCs

To directly investigate whether *C. cateniformis* affects immune function by downregulating PD-L2 expression or whether PD-L2 expression is a marker for other immunological activities, we transduced BMDCs with lentivirus expressing either GFP or GFP and PD-L2 (PD-L2-GFP) (Extended Data Fig. 7k). GFP BMDCs pretreated with soluble *C. cateniformis* surface extracts in vitro stimulated OT-I CD8⁺ T cells to express increased IFN γ , TNF, CD107a, granzyme B, CD44 and CD25 compared with vehicle control DCs. This result indicates that *C. cateniformis* treatment of BMDCs promotes an increased proinflammatory CD8⁺ T cell response in vitro (Fig. 3b–d and Extended Data Fig. 7l–p). Conversely, pretreatment of PD-L2-GFP BMDCs with *C. cateniformis* extract did not have these effects. IFN γ , TNF, CD107a and CD44 expression were not increased, granzyme B was modestly increased and CD25 expression was similarly increased (Fig. 3b–d and Extended Data Fig. 7l–p). These data show that many of the immunomodulatory effects of *C. cateniformis* can be negated by forced PD-L2 expression, which is consistent with the idea that *C. cateniformis*-mediated downregulation of PD-L2 expression is the mechanism by which this microbe enhances anti-PD-L1 therapy.

When *C. cateniformis* was orally gavaged at the time that anti-PD-L1 treatment was given, the resulting anti-tumour response was as strong as with combined anti-PD-L1 and anti-PD-L2 therapy in antibiotic-treated mice. The combination of *C. cateniformis*, anti-PD-L1 and anti-PD-L2 treatment did not further enhance the anti-tumour response, which suggests that *C. cateniformis* and anti-PD-L2 have overlapping mechanisms of action (Extended Data Fig. 8a).

To determine whether the anti-tumour properties of *C. cateniformis* depend on the suppression of PD-L2 expression on DCs, we transferred GFP or GFP-PD-L2 BMDCs into B16-OVA tumours in GF mice and in mice monocolonized with *C. cateniformis* 3 days after tumour implantation. GFP BMDCs promoted significantly stronger anti-tumour responses in *C. cateniformis* monocolonized mice compared with GF mice, which provides support for our hypothesis that *C. cateniformis* enhances DC-mediated anti-tumour immunity (Fig. 3e). Notably, transfer of PD-L2-overexpressing DCs resulted in significantly larger tumour volumes compared with transfer of GFP DCs in *C. cateniformis* monocolonized GF mice (Fig. 3e) and SPF mice (Extended Data Fig. 8b). This result indicates that high levels of PD-L2 expression on DCs inhibit anti-tumour immunity. The anti-tumour properties of *C. cateniformis* depend on PD-L2 downregulation, as *C. cateniformis* could not promote strong anti-tumour immunity in the presence of high PD-L2. Thus, our in vitro and in vivo data demonstrate that the anti-tumour effects of *C. cateniformis* depend on downregulation of PD-L2 expression on DCs.

To directly show that *C. cateniformis* promotes anti-tumour immunity through the downregulation of PD-L2 on DCs, we implanted wild-type (WT) or *Pdl2* knockout (KO) DCs with or without *C. cateniformis* treatment into tumour sites in SPF mice with B16-OVA tumours. Because our data showed that transfer of GFP BMDCs promoted strong anti-tumour immunity in SPF mice (Extended Data Fig. 8b), we sought to find a BMDC transfer model in which WT BMDC transfer was less efficacious and thus could be enhanced by PD-L2 suppression. We proposed that less mature BMDCs that had been cultured for 6–7 days, and therefore express lower levels of MHCII compared with more mature BMDCs that had been cultured for 10 days (Extended Data Fig. 8c–e and Fig. 3e), would be less immunostimulatory. Although transfer of day 6 cultured WT BMDCs slightly delayed B16-OVA tumour growth, by day 20 there was no significant difference between no transfer and WT BMDC transferred tumours (Fig. 3f). Injection of WT BMDC pretreated with *C. cateniformis* extract, however, was sufficient to promote a strong anti-tumour response. This result indicates that the immunomodulatory impact of *C. cateniformis* on DCs is sufficient to promote anti-tumour immunity. Notably, transfer of *Pdl2* KO DCs promoted a strong anti-tumour response that could not be further enhanced by pretreatment with *C. cateniformis*.

extract (Fig. 3f). These data indicate that inhibition of PD-L2 expression on DCs plays a key part in promoting anti-tumour immunity and that *C. cateniformis* treatment cannot enhance anti-tumour immunity independent of PD-L2 downregulation.

Targeting PD-L2–RGMb interactions

Based on our observation that combined blockade of PD-1 and PD-L2 gave better anti-tumour responses than PD-1 blockade alone (Extended Data Fig. 3a), we proposed that the PD-L2 effect is mediated by a receptor other than PD-1. Consequently, we investigated whether the interaction of PD-L2 with RGMb rather than PD-1 led to microbiome-dependent resistance to anti-PD-L1 or anti-PD-1 cancer therapy. We tested whether blocking the PD-L2–PD-1 interaction or the PD-L2–RGMb interaction was necessary to promote an anti-tumour response to PD-L1 blockade. To that end, we compared the effects of two functionally distinct PD-L2 blocking antibodies in combination with anti-PD-L1 in GF mice and in antibiotic-treated mice. The 2C9 anti-PD-L2 clone selectively blocks the RGMb–PD-L2 interaction, whereas the 3.2 anti-PD-L2 clone blocks both RGMb–PD-L2 and PD-1–PD-L2 interactions^{19,20} (Fig. 4a). Monotherapy with anti-PD-L1 or either anti-PD-L2 clone did not suppress MC38 tumour growth in antibiotic-treated mice or GF mice. By contrast, administration of either the 3.2 clone or the 2C9 clone together with anti-PD-L1 (Fig. 4b,c) or anti-PD-1 (Fig. 4d) induced a strong anti-tumour response in antibiotic-treated mice and GF mice. This result demonstrates that blockade of the PD-L2 interaction with RGMb is sufficient to promote an anti-tumour response to PD-1 or PD-L1 blockade. Similarly, anti-PD-L1 and either anti-PD-L2 antibody reduced the growth of the less immunogenic B16-OVA tumour (Fig. 4e). *B2m*^{−/−} mice, which lack CD8⁺ T cells, implanted with MC38 tumour cells failed to respond to combined treatment with anti-PD-L1 and the 2C9 anti-PD-L2 clone (Extended Data Fig. 8f). This result suggests that CD8⁺ T cells are needed for the anti-tumour response to this combination treatment.

Next we investigated the effects of combined administration of an anti-RGMb monoclonal antibody and an anti-PD-L1 or anti-PD-1 treatment in the MC38 tumour model in GF mice. Anti-RGMb (9D1 clone¹⁹) attenuated tumour growth in GF mice when given with either anti-PD-L1 or anti-PD-1 (Fig. 4f,g). This was in contrast to the poor response to anti-RGMb, anti-PD-L1 or anti-PD-1 alone. Anti-PD-L1 combined with either an anti-PD-L2 antibody or an anti-RGMb antibody similarly promoted a strong anti-tumour response in GF mice with MC38 tumours (Extended Data Fig. 8g) as well as in Taconic SPF mice with B16-OVA tumours (Extended Data Fig. 8h). To determine whether the anti-RGMb antibody exerts its anti-tumour effects by blocking pathway activity or by depleting cells, we compared the recombinant anti-RGMb 9D1 antibody with a WT (mouse IgG2a) or effectorless crystallizable fragment (Fc; mouse IgG2a-LALA-PG), in which the Fc portion is not able to bind to the Fc receptor and therefore cannot function to deplete RGMb⁺ cells. Both RGMb antibodies attenuated tumour growth in antibiotic-treated mice treated with anti-PD-L1, and significantly increased survival compared with anti-PD-L1 therapy alone. This result indicates that RGMb blockade is sufficient to induce an anti-tumour response and that depletion of RGMb⁺ cells is not part of the mechanism (Fig. 4h,i). It is notable that anti-PD-1 therapy benefits from combination with anti-PD-L2 and that either PD-1 or PD-L1 blockade combined with the anti-PD-L2 2C9 clone or anti-RGMb promotes as strong an anti-tumour effect as when combined with the anti-PD-L2 3.2 clone. These findings demonstrate that the RGMb–PD-L2 pathway plays an important part in limiting the response to anti-PD-1 or anti-PD-L1 immunotherapy in a GF or colonized host.

The microbiota affects RGMb expression

To further understand how the gut microbiota regulates the RGMb–PD-L2 interaction, we compared RGMb expression in SPF and GF mice

bearing MC38 tumours. RGMb is expressed in the nervous system, epithelial cells and immune system, in which it is most highly expressed by macrophages^{19,21,22}. Notably, the transcript levels of *Rgmb* in CD8⁺ tumour-infiltrating T cells were 6.1-fold higher in GF mice compared with SPF mice (Fig. 5a). Similarly, RGMb protein expression, measured by a monoclonal antibody (9D3 clone) or a polyclonal antibody (Fig. 5b and Extended Data Fig. 9a–d), was significantly higher in CD8⁺ tumour-infiltrating T cells from GF mice compared with SPF mice. Differences in RGMb expression in other immune cell subsets were not significant (Fig. 5b), which suggests that RGMb expression on T cells plays an important part in CD8⁺ T-cell-mediated anti-tumour immunity. At day 29 after tumour implantation, analyses of mice colonized with human stool samples revealed that tumours from NR2-colonized mice had significantly higher expression of RGMb on CD8⁺ T cells but not on CD11b⁺ or CD11c⁺ DCs. This result suggests that certain NR patients might have a microbiota that result in increased RGMb expression on T cells (Extended Data Fig. 9e–g). Moreover, there were significantly fewer RGMb-expressing intratumoural CD8⁺ T cells in SPF mice treated with an anti-PD-L1 or isotype antibody compared with GF mice treated with an anti-PD-L1 or isotype antibody (Fig. 5c). MC38 tumour cells expressing GFP showed high expression of PD-L1, as previously reported²³, but undetectable RGMb or PD-L2 expression when implanted in SPF or GF mice. This result suggests that RGMb or PD-L2 expression on immune cells and not the tumour is responsible for influencing anti-tumour immunity (Extended Data Fig. 9h). Taken together, these findings demonstrate that blockade of PD-L2–RGMb interactions can overcome microbiome-dependent resistance to anti-PD-1 or anti-PD-L1 therapy.

RGMb functions on T cells

To determine how anti-RGMb treatment affects immune responses in GF mice, we analysed immune cell subsets at day 18 after MC38 tumour implantation. Combined anti-PD-L1 and anti-RGMb therapy in GF mice led to a significant increase in the numbers of intratumoural CD8⁺ and CD4⁺ T cells compared with mice treated with isotype controls (Fig. 5d,e). Anti-PD-L1 treatment alone did not significantly change the numbers of intratumoural CD8⁺ and CD4⁺ T cells in GF mice, which is consistent with previous findings¹⁵. The numbers of intratumoural T_{reg} cells were similar in GF mice given anti-PD-L1, anti-PD-L1 plus anti-RGMb or isotype control antibody. Consequently, the CD8⁺ to T_{reg} cell ratio was increased in the tumours of GF mice treated with anti-PD-L1 and anti-RGMb antibodies (Fig. 5f,g). Even as early as day 11 after tumour implantation, anti-RGMb combined with anti-PD-L1 treatment significantly increased TNF production by CD4⁺ T cells (Extended Data Fig. 9i), which indicates that RGMb has a potential role in the regulation of pro-inflammatory cytokine expression by T cells. PD-1 expression on CD8⁺ tumour-infiltrating T cells was increased in mice treated with anti-RGMb without upregulation of the co-inhibitory receptors TIM-3 and LAG-3 (Extended Data Fig. 9j–l). These data suggest that combined anti-PD-L1 and anti-RGMb treatment acts on T cells to enhance anti-tumour immunity.

To directly investigate the function of RGMb on specific cell types in the regulation of anti-tumour immunity, we developed *Rgmb* conditional KO mice (*Rgmb*^{fl/fl}) and crossed them with CD4-Cre to delete RGMb in T cells or with LysM-Cre mice to delete RGMb in macrophages and granulocytes (Extended Data Fig. 9m–o). Deletion of *Rgmb* in T cells, but not macrophages and granulocytes, improved anti-tumour responses in antibiotic-treated mice given anti-PD-L1 (Fig. 5h,i). Furthermore, in co-cultures of WT BMDCs with WT or *Rgmb* KO CD8⁺ T cells, the *Rgmb* KO T cells displayed a more activated phenotype, with increased mean fluorescence intensity of CD44 (Fig. 5j), T-bet and a slight but not significant increase of CD107a (Extended Data Fig. 9p,q). Moreover, there were significantly increased percentages of RGMb KO CD8⁺ T cells expressing IFN γ , IL-2 and TNF (Fig. 5k). Both sets of T cells had high

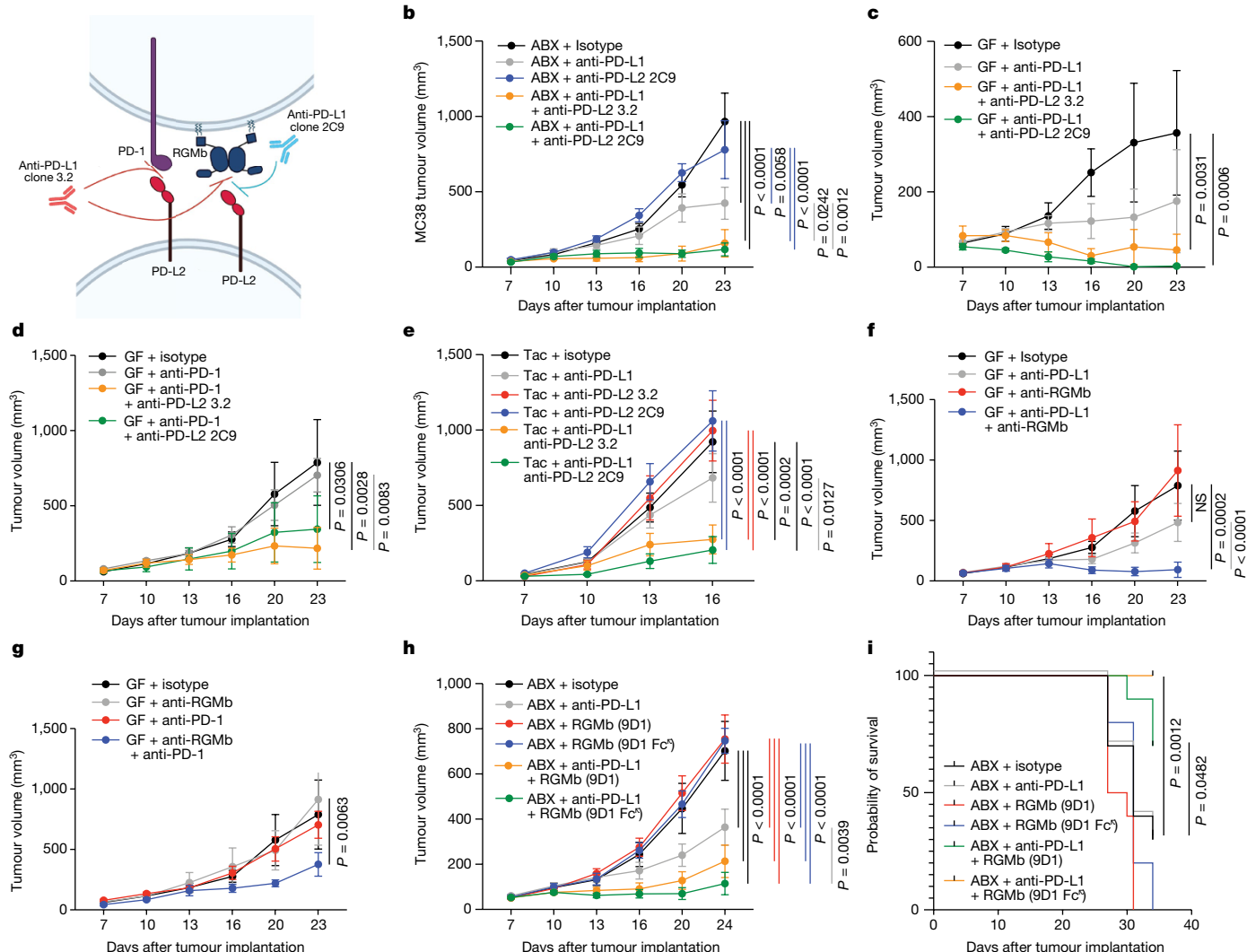


Fig. 4 | PD-L2-RGMB blockade is sufficient to promote anti-tumour responses in mice that do not respond to anti-PD-1 or anti-PD-L1 treatment alone. **a**, Diagram of PD-L2 binding to PD-1 or RGMB, and blocking specificity of anti-PD-L2 antibodies. Anti-PD-L2 clone 3.2 blocks both PD-L2-PD-1 and PD-L2-RGMB interactions. Anti-PD-L2 clone 2C9 blocks only the PD-L2-RGMB interaction¹⁹. **b,c**, MC38 tumour growth in ABX-treated mice (**b**; $n = 5$ mice per group for all groups except for the anti-PD-L2 2C9 group, where $n = 4$ mice) and in GF mice (**c**; $n = 5$ mice per group). Data representative of two to three experiments. **d**, MC38 tumour growth in GF mice given an isotype ($n = 4$ mice), anti-PD-1 ($n = 5$ mice) or anti-PD-1 antibody combined with either of the anti-PD-L2 clones ($n = 5$ mice per group). **e**, B16-OVA tumour growth in Taconic (Tac) SPF mice given an isotype ($n = 10$ mice), anti-PD-L1 ($n = 10$ mice), anti-PD-L2 3.2 ($n = 10$ mice), anti-PD-L2 2C9 ($n = 10$ mice) or anti-PD-L1 antibody with either of the anti-PD-L2 clones ($n = 9$ mice each). Data representative of three experiments. **f**, MC38 tumour growth in GF mice and treated with an isotype ($n = 4$ mice),

anti-RGMB ($n = 4$ mice), anti-PD-L1 ($n = 5$ mice) or anti-PD-L1 plus anti-RGMB ($n = 5$ mice) antibody. Data representative of two experiments. **g**, MC38 tumour growth in GF mice and treated with an isotype ($n = 4$ mice), anti-RGMB ($n = 4$ mice), anti-PD-1 ($n = 5$ mice) or anti-PD-1 plus anti-RGMB ($n = 5$ mice) antibody. Data representative of two experiments. **h**, MC38 tumour growth in ABX-treated mice treated with an isotype, anti-RGMB (mIgG2a), anti-RGMB (mIgG2a-LALA-PG, termed Fc^o), anti-PD-L1, anti-PD-L1 plus anti-RGMB (mIgG2a), or anti-PD-L1 plus anti-RGMB (Fc^o) antibody. $n = 10$ mice per group. **i**, Corresponding survival curves of data from **h**. Significance between anti-PD-L1 versus anti-PD-L1 with either of the anti-RGMB antibodies determined using log-rank (Mantel-Cox) test. For **b-h**, significance was determined using two-way ANOVA with Tukey's multiple comparisons test, and error bars show the mean and s.e.m. Panel **a** was created using BioRender (<https://www.biorender.com>).

levels of proliferation and granzyme B mean fluorescence intensity, but were not significantly different (Extended Data Fig. 9r,s). Together, these findings reveal a new, inhibitory function for RGMB on T cells and provide a deeper mechanistic understanding of the role of RGMB in anti-tumour immunity.

Discussion

Current understanding of how the gut microbiota can enhance cancer immunotherapy is still at an early stage. Faecal microbiota transplantation studies have shown that the efficacy of anti-PD-1 therapy

can be increased by 30% in patients^{7,8}, but probiotics did not enhance patient survival. In fact, an inverse correlation between the use of probiotics and anti-PD-L1 response has been reported²⁴. There are multiple ways that gut bacteria can promote anti-tumour immunity. For example, different bacteria can secrete inosine⁵, a hydrolase that generates muropeptides⁶, or STING agonists that enhance the response to immunotherapy¹⁴. Further work is needed to define mechanisms by which the gut microbiota enables the adaptive immune system to overcome the immunosuppressive tumour microenvironment.

By investigating immune responses in microbiome-dependent mouse cancer models, we discovered a new mechanism by which the

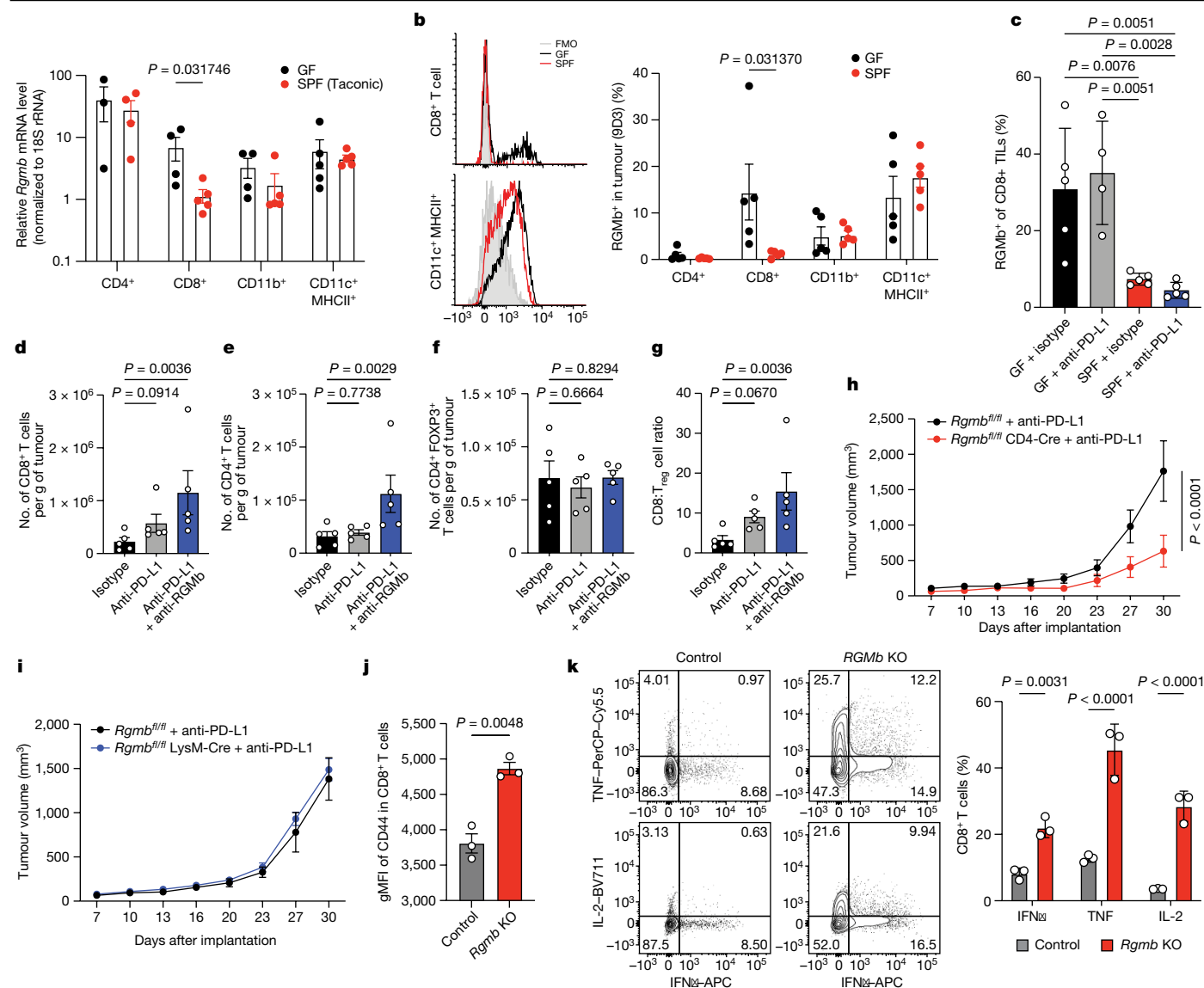


Fig. 5 | RGMB on T cells regulates anti-tumour immunity. **a**, *Rgmb* RNA expression in CD4⁺ T cells ($n = 3$ tumours from GF mice, $n = 4$ tumours from SPF mice), CD8⁺ T cells ($n = 4$ GF mice, $n = 5$ SPF mice), CD11c⁺MHCII⁺ cells ($n = 5$ GF mice and SPF mice) and CD11b⁺ cells ($n = 4$ GF mice, $n = 5$ SPF mice) sorted from tumours on day 11 after implantation (RNA levels quantified using reverse transcription quantitative real-time PCR). **b**, Representative histograms of RGMB (RGMB-Alexa 594 clone 9D3) surface expression on CD8⁺ T cells (top left) and CD11c⁺MHCII⁺ cells (bottom left) in GF mice and SPF mice. RGMB⁺ cell frequencies were also quantified (right). $n = 5$ mice per group. FMO, fluorescence minus one, CD8⁺ T cell RGMB expression on day 11 after tumour implantation. $n = 5$ mice GF plus isotype and SPF groups, $n = 4$ mice GF plus anti-PD-L1. Significance determined using one-way ANOVA and Sidak's multiple comparisons test. **d–g**, Numbers of CD8⁺ T cells (**d**), CD4⁺ T cells (**e**) and

Treg cells (**f**) in GF mouse tumours at day 18 after implantation. **g**, Ratio of CD8⁺ to Treg cells. Significance calculated using nonparametric one-way ANOVA and Dunn's multiple comparisons test, $n = 5$ mice per group. **h, i**, Tumour growth in *Rgmb*^{+/+} ($n = 8$ mice) and *Rgmb*^{+/+} CD4-Cre ($n = 10$ mice) mice (**h**) *Rgmb*^{+/+} ($n = 7$ mice) and *Rgmb*^{+/+} LysM-Cre ($n = 12$ mice) mice (**i**) treated with ABX and anti-PD-L1. Day 30 significance determined using two-way ANOVA and Sidak's multiple comparisons test. **j, k**, OVA-pulsed WT BMDCs were co-cultured with WT or *Rgmb* KO OT-I CD8⁺ T cells. Geometric mean fluorescence intensity (gMFI) of CD44 (**j**) and frequency of cells expressing IFN γ , TNF and IL-2 (**k**). For **a, b, j** and **k**, significance was calculated using unpaired, two-tailed, Mann-Whitney test. Error bars show the mean and s.d. for bar graphs and the mean and s.e.m. for tumour graphs. For all graphs, representative data from two experiments are shown and tumours were MC38.

microbiota can promote responses to anti-PD-1 and anti-PD-L1 therapy, whereby PD-L2 and RGMB expression on immune cells is downregulated in responder mice. Upregulated expression of PD-L2 and RGMB in non-responder GF mice or antibiotic-treated mice is functionally significant because blockade of the PD-L2–RGMB pathway (using either anti-PD-L2 or anti-RGMB antibodies) combined with anti-PD-1 or anti-PD-L1 treatment promotes anti-tumour responses in GF mice and in antibiotic-treated mice that do not respond to anti-PD-1 or anti-PD-L1 alone. The requirement for RGMB or PD-L2 blockade to potentiate the effect of PD-1 blockade in GF mice suggests that the

PD-L2 inhibitory effect may be largely through RGMB–PD-L2 interactions and not PD-1–PD-L2 interactions. Combined anti-PD-L1 and anti-PD-L2 therapy enhanced tumour clearance and survival compared with monotherapy in mice colonized with stool from NR patients. This result suggests that this combination therapy may have translational relevance, particularly in patients with a non-responder microbiota.

Monocolonization with *C. cateniformis* was sufficient to promote a response to anti-PD-L1 therapy and suppress PD-L2 expression on DCs in MLNs and tumour dLNs. Our data suggest that this signal could originate in the MLNs and travel to tumour dLNs. Notably, incubation

of BMDCs with *C. cateniformis* surface extracts suppressed PD-L2 expression, and injection of *C. cateniformis*-treated WT BMDCs or *Pdl2* KO BMDCs promoted a strong anti-tumour response compared with controls. Conversely, transfer of PD-L2-overexpressing BMDCs resulted in significantly larger tumours than WT BMDC transfer in *C. cateniformis*-colonized mice. Together, these studies demonstrate that PD-L2 expression on DCs plays a key part in limiting anti-tumour immunity and that *C. cateniformis* promotes anti-tumour immunity by downregulating PD-L2 expression on DCs. Our finding that *Pdl2* KO DCs strongly promote an anti-tumour response suggests a new strategy for cellular therapy. Previous studies have shown that bacteria from different phyla can have overlapping immunoregulatory consequences, and strains of the same species can produce different immunoregulatory outcomes. Consequently, *C. cateniformis* is probably not the only strain in the human microbiota that can mediate this effect²⁵. We isolated a second organism that also promoted anti-tumour immunity to anti-PD-L1 but did not significantly suppress PD-L2. Therefore, although PD-L2 suppression by some bacteria can promote anti-tumour immunity, this is not the only mechanism by which gut microbes can affect immune function during immunotherapy.

RGMb is expressed by several cell types, including neuronal cells, epithelial cells and immune cells^{21,22,26}. In the immune system, RGMb has been implicated in mucosal tolerance and asthma^{19,27}. RGMb has an important role in neuronal development and kidney function. Moreover, global conditional *Rgmb* KO can alter the gut microbiome and increase susceptibility to colitis induced by dextran sulfate sodium²⁸. Thus, the PD-L2–RGMb axis may be a key mediator of tolerogenic interactions between the microbiota and the host immune system. Our work using *Rgmb* conditional KO mice lacking RGMb only on T cells revealed a previously unknown role for RGMb on T cells in anti-tumour immunity. Previous studies have focused on RGMb function on DCs and myeloid cells^{19,27}.

In conclusion, by investigating how the gut microbiome modulates anti-tumour immunity, we identified attenuation of PD-L2 and RGMb expression as an immunoregulatory mechanism that informs a possible therapeutic strategy to overcome resistance to PD-1 blockade. We propose a two-step model in which certain gut bacteria suppress PD-L2 expression on DCs in lymph nodes, and PD-L2^{lo} DCs play a crucial part in activating CD8⁺ T cells to promote anti-tumour immunity. By contrast, PD-L2^{high} DCs interact with RGMb on CD8⁺ T cells to inhibit CD8⁺ T cell responses. RGMb expression is maintained at a low level in the tumour microenvironment of a host with a favourable gut microbiota, whereas unfavourable gut microbiota may induce upregulation on CD8⁺ tumour-infiltrating lymphocytes. Blockade of PD-L2–RGMb interactions combined with anti-PD-1 or anti-PD-L1 therapy can overcome microbiome-dependent resistance to monotherapies with PD-1 pathway inhibitors and provides a new strategy for treating patients who do not respond to PD-1 cancer immunotherapy. Our study provides an innovative approach to identify new cancer immunotherapy targets using the gut microbiome as a discovery platform.

Online content

Any methods, additional references, Nature Portfolio reporting summaries, source data, extended data, supplementary information,

acknowledgements, peer review information; details of author contributions and competing interests; and statements of data and code availability are available at <https://doi.org/10.1038/s41586-023-06026-3>.

- Vétizou, M. et al. Anticancer immunotherapy by CTLA-4 blockade relies on the gut microbiota. *Science* **350**, 1079–1084 (2015).
- Routy, B. et al. Gut microbiome influences efficacy of PD-1–based immunotherapy against epithelial tumors. *Science* **359**, 91–97 (2018).
- Sivan, A. et al. Commensal *Bifidobacterium* promotes antitumor immunity and facilitates anti-PD-L1 efficacy. *Science* **350**, 1084–1089 (2015).
- Tanoue, T. et al. A defined commensal consortium elicits CD8 T cells and anti-cancer immunity. *Nature* **565**, 600–605 (2019).
- Mager, L. F. et al. Microbiome-derived inosine modulates response to checkpoint inhibitor immunotherapy. *Science* **369**, 1481–1489 (2020).
- Griffin, M. E. et al. *Enterococcus* peptidoglycan remodeling promotes checkpoint inhibitor cancer immunotherapy. *Science* **373**, 1040–1046 (2021).
- Baruch, E. N. et al. Fecal microbiota transplant promotes response in immunotherapy-refractory melanoma patients. *Science* **371**, 602–609 (2021).
- Davar, D. et al. Fecal microbiota transplant overcomes resistance to anti-PD-1 therapy in melanoma patients. *Science* **371**, 595–602 (2021).
- Ribas, A. & Wolchok, J. D. Cancer immunotherapy using checkpoint blockade. *Science* **359**, 1350–1355 (2018).
- Zhao, B., Zhao, H. & Zhao, J. Efficacy of PD-1/PD-L1 blockade monotherapy in clinical trials. *Ther. Adv. Med. Oncol.* **12**, 1758835920937612 (2020).
- Chung, H. et al. Gut immune maturation depends on colonization with a host-specific microbiota. *Cell* **149**, 1578–1593 (2012).
- Surana, N. K. & Kasper, D. L. Moving beyond microbiome-wide associations to causal microbe identification. *Nature* **552**, 244–247 (2017).
- Fransen, M. F. et al. Tumor-draining lymph nodes are pivotal in PD-1/PD-L1 checkpoint therapy. *JCI Insight* <https://doi.org/10.1172/jci.insight.124507> (2018).
- Lam, K. C. et al. Microbiota triggers STING-type I IFN-dependent monocyte reprogramming of the tumor microenvironment. *Cell* **184**, 5338–5356 (2021).
- Gopalakrishnan, V. et al. Gut microbiome modulates response to anti-PD-1 immunotherapy in melanoma patients. *Science* **359**, 97–103 (2018).
- Matson, V. et al. The commensal microbiome is associated with anti-PD-1 efficacy in metastatic melanoma patients. *Science* **359**, 104–108 (2018).
- Kageyama, A. & Benno, Y. *Coprobacillus cateniformis* gen. nov., sp. nov., a new genus and species isolated from human feces. *Microbiol. Immunol.* **44**, 23–28 (2000).
- Silveira-Nunes, G. et al. Hypertension is associated with intestinal microbiota dysbiosis and inflammation in a Brazilian population. *Front. Pharmacol.* **11**, 258 (2020).
- Xiao, Y. et al. RGMb is a novel binding partner for PD-L2 and its engagement with PD-L2 promotes respiratory tolerance. *J. Exp. Med.* **211**, 943–959 (2014).
- Pauken, K. E., Torchia, J. A., Chaudhri, A., Sharpe, A. H. & Freeman, G. J. Emerging concepts in PD-1 checkpoint biology. *Semin. Immunol.* **52**, 101480 (2021).
- Severyn, C. J., Shinde, U. & Rotwein, P. Molecular biology, genetics and biochemistry of the repulsive guidance molecule family. *Biochem. J.* **422**, 393–403 (2009).
- Xia, Y. et al. Dragon (repulsive guidance molecule b) inhibits IL-6 expression in macrophages. *J. Immunol.* **186**, 1369–1376 (2011).
- Juneja, V. R. et al. PD-L1 on tumor cells is sufficient for immune evasion in immunogenic tumors and inhibits CD8 T cell cytotoxicity. *J. Exp. Med.* **214**, 895–904 (2017).
- Spencer, C. N. et al. Dietary fiber and probiotics influence the gut microbiome and melanoma immunotherapy response. *Science* **374**, 1632–1640 (2021).
- Geva-Zatorsky, N. et al. Mining the human gut microbiota for immunomodulatory organisms. *Cell* **168**, 928–943.e11 (2017).
- Xia, Y. et al. Dragon enhances BMP signaling and increases transepithelial resistance in kidney epithelial cells. *J. Am. Soc. Nephrol.* **21**, 666–677 (2010).
- Yu, S. et al. Blockade of RGMb inhibits allergen-induced airways disease. *J. Allergy Clin. Immunol.* **144**, 94–108.e11 (2019).
- Shi, Y. et al. Repulsive guidance molecule b deficiency induces gut microbiota dysbiosis and increases the susceptibility to intestinal inflammation in mice. *Front. Microbiol.* **12**, 648915 (2021).

Publisher's note Springer Nature remains neutral with regard to jurisdictional claims in published maps and institutional affiliations.

Springer Nature or its licensor (e.g. a society or other partner) holds exclusive rights to this article under a publishing agreement with the author(s) or other rightsholder(s); author self-archiving of the accepted manuscript version of this article is solely governed by the terms of such publishing agreement and applicable law.

© The Author(s), under exclusive licence to Springer Nature Limited 2023

Methods

Mice

C57BL/6 female mice (6 weeks old) were purchased from Taconic Biosciences. β 2m-deficient mice were obtained from the Jackson Laboratory. Mice were randomly assigned to different treatment groups, and experiments were performed blinded when possible. GF mice were maintained in the GF facility at Harvard Medical School. All experimental mice were housed in specific pathogen-free conditions or GF isolators. *Rgmb* conditional KO mice were generated by homologous integration of a construct, which contains *loxP* sites flanking exon 2 of the *Rgmb* gene and a neomycin cassette in C57BL/6 embryonic stem cells (Extended Data Fig. 9m). Neo flanked by *Frt* sites was removed by breeding mice with germline transmission of the homologously integrated construct with a *Flp* deleter strain. *Rgmb* conditional KO mice were further crossed with LysM-Cre (Jackson Laboratory, 004781) or CD4-Cre mice (Jackson Laboratory, 022071) to generate macrophage-specific or T-cell-specific conditional KO mice, respectively. All mice were used in accordance with animal care guidelines from the Harvard Medical School Standing Committee on Animals and the National Institutes of Health. Mice were housed by the facilities operated by the Harvard Center for Comparative Medicine under the following housing conditions: 12–12 h light–dark cycle, main room temperature of 20–26 °C and humidity of 40–65%. All mice were used in accordance with animal care guidelines from the Harvard Medical School Standing Committee on Animals and the National Institutes of Health.

Tumour models and antibody treatment

Mice were anaesthetized with 2.5% 2,2,2-tribromoethanol (avertin, Sigma Aldrich, T48402-25G) diluted in DPBS and subcutaneously injected in the abdominal flank with 2.5×10^5 MC38 tumour cells, B16-OVA tumour cells, or LLC-OVA, MB49 or Py8119-OVA cells. Alternatively, 2.5×10^5 E0771 cells were injected into the mammary fat pad. Whenever GF mice or antibody-treated mice were directly compared with SPF mice, HMB-treated mice or ABX/HMB-treated mice, tumour cells from the same cultures were implanted into all groups of mice on the same day. Mice were given the following antibodies intraperitoneally individually or in combination as indicated on days 7, 10, 13 and 16 after tumour implantation: 100 μ g of anti-PD-L1 antibody (clone 10F.9G2), anti-PD-1 antibody (clone RMP1-14), anti-PD-L2 antibody (clone 3.2), anti-PD-L2 antibody (clone GF17.2C9), anti-RGMb antibody (clone 307.9D1), recombinant anti-RGMb antibody (clone 307.9D1), Fv with either WT mouse IgG2a Fc or L234A/L235A/P329G (LALA-PG) triple mutant Fc effector silent antibody²⁹, rat IgG2b isotype control (LTF-2, BioXCell, BE0090) or rat IgG2a isotype control (2A3 BioXCell, BE0089). Antibodies 10F.9G2, RMP1-14, 29F.1A12 and 3.2 are commercially available for research purposes. Antibodies 307.9D1 and GF17.2C9 are available for distribution to investigators at academic institutions for research purposes using standard academic material transfer agreements. Requests from for-profit corporations will require negotiation of an appropriate licensing agreement with the technology transfer office of the institution. Tumour volume was determined by the volume formula for an ellipsoid: $0.5 \times D \times d^2$, where D is the longer diameter and d is the shorter diameter. Mice were humanely euthanized when tumours were ulcerated or reached the volume of 2,000 mm³ in accordance with our institutional animal care and use committee protocol.

Antibiotic treatment and faecal transfer

Antibiotics were given through drinking water. For broad-spectrum antibiotic treatment, 0.5 mg ml⁻¹ of vancomycin, 1 mg ml⁻¹ of neomycin, 1 mg ml⁻¹ of metronidazole and 1 mg ml⁻¹ of ampicillin were added to drinking water containing Splenda (4 g l⁻¹). Antibiotic water was refreshed every 3 days. To confirm antibiotic activity, faecal matter was resuspended in PBS (1 ml per pellet) and cultured on Trypticase soy agar

and Brucella blood agar plates in aerobic and anaerobic conditions, respectively. For HMB or MMB treatments, colon contents from ten C57BL/6 HMB-treated mice or MMB-treated mice^{11,12} were squeezed into a pre-weighed 50 ml tube and resuspended in brain heart infusion medium at 100 mg ml⁻¹ in an anaerobic chamber. Aliquots were kept at -80 °C. GF mice were orally gavaged with 200 μ l of HMB or MMB stock 1 week before tumour implantation. For ABX/HMB-treated mice, treatment with antibiotics was stopped at day 7 after implantation, and mice were orally gavaged with 200 μ l of HMB stock^{11,12}. For individual antibiotic experiments, mice were treated with broad-spectrum antibiotics until day 7 after tumour implantation, at which point they were orally gavaged with HMB and continued with only a single antibiotic in the drinking water until the end of the experiment.

Patient stool samples

For in vivo studies involving human samples, stool samples were obtained from patients with melanoma treated with immune checkpoint blockade (ICB; anti-PD-1). Fresh frozen faecal samples were used, including one responder (CR, sample identifier 274 (ref. 14) and two non-responders (NR1, sample identifier 376 (unpublished observations) and NR2, sample identifier 426 (ref. 14)). Patients were selected on the basis of their tumour progression and overall survival after surgery and subsequent treatment with PD-1 blockade (pembrolizumab or nivolumab). Response to treatment was assessed by radiographical imaging and according to the response evaluation criteria in solid tumours (RECIST 1.1)³⁰. Patients with complete or partial response or stable disease ≥ 6 months were classified as responders, and those with stable disease <6 months or progressive disease were classified as non-responders. The mean patient age was 56.3 years (50–62 years), and mean body-mass index was 29.9 kg m⁻² (20.4–42.31 kg m⁻²). The CR sample was taken 2 years after treatment. Complete response was identified 3 years before faecal sample collection. The non-responder samples were taken during treatment, 3 months to 1 year after the start of ICB. Samples were collected under approved institutional review board protocols 2012-0846 and PA15-0232. Fresh stool samples were collected in stool collection cups, shipped overnight on ice to the Melanoma Clinical Database, Tissue Resource and Translational Pathology Core at the University of Texas MD Anderson Cancer Center. Samples were then aliquoted and stored at -80 °C.

Faecal microbiota transplantation tumour studies

For faecal microbiota transplantation studies, stool samples were prepared in an anaerobic chamber. One gram of stool was diluted in 10 ml PBS and 10% glycerol. Diluted stool samples were filtered using a 100 μ m cell strainer, aliquoted and stored at -80 °C. Next 200 μ l of diluted patient stool was administered to mice by oral gavage 8, 6 and 4 days before tumour implantation.

16S sequencing of mouse stool

DNA from frozen stool samples was extracted using a QIAamp Fast DNA Stool Mini kit (Qiagen, 51604) for Extended Data Fig. 5 or by phenol–chloroform extraction as previously published³¹ for Extended Data Fig. 9. Purified DNA was quantified using a Qubit dsDNA HS assay (Thermo Fisher, Q32854) and normalized. The V4 region of the 16S rRNA gene was amplified with primers 515F and 806R as previously described³², and around 390 bp amplicons were purified and quantified using a Qubit dsDNA HS assay and combined with equal mass to make a pooled library. The pooled library was multiplexed and sequenced (Illumina MiSeq, 251 nt \times 2 pair-end reads with 12 nt index reads) at the Harvard Biopolymers Facility. Raw sequencing data were processed using QIIME2 pipelines³³. In brief, raw sequencing data were imported into QIIME2 and demultiplexed, then DADA2 was used for sequence, quality control and feature table construction. The feature table was further used for beta diversity analysis, taxonomic analysis and differential abundance testing using QIIME2. We used QIIME2_DADA2

to convert raw sequencing data into Amplicon Sequencing Variant ASV-level feature identification, and then performed differential abundance testing on all different taxonomy levels. We then focused on the genus level because of the resolution limitation of the 16S V4 region. We identified a total of five genera significantly associated with response to anti-PD-L1 groups with an abundance ratio (R/NR) over 5. Beta group significance was determined by permutational analysis of variance. Identification of taxa associated with different groups was determined using analysis of composition of microbiomes.

Isolation of Gram-positive strains from HMB

Isolation of Gram-positive strains from HMB was performed in an anaerobic chamber. Faeces from HMB-treated mice were collected and resuspended in PBS at 100 mg ml⁻¹. Serial dilutions of HMB stock were plated on brain heart infusion plates made according to the manufacturer's instructions (BD, 241830) and stored in an anaerobic chamber for 3 days. Individual isolates were selected from these plates and cultured in reinforced clostridial medium (BD, 218081) overnight in an anaerobic chamber. Stocks were made from overnight cultures, diluted so that they contained 20% glycerol and stored at -80 °C. Stocks were plated on BD BBL Brucella plates (BD, 8807311) in an anaerobic chamber to confirm viability, and colonies were sequenced to identify strains. Individual colonies were resuspended in 50 µl of DMSO and heated at 95 °C for 15 min and quickly spun down to access bacterial DNA. For PCR of full-length 16S bacteria sequences, 2 µl of bacterial DNA was mixed with 10 µl 5× GC buffer (New England BioLabs, B0519S) and 1 µl of 1 µM dNTPs and 2.5 µl each of 10 µM forward (27F, AGA GTT TGA TCM TGG CTC AG) and reverse primers (1492R, CGG TTA CCT TGT TAC GAC TT) and 1 µl Phusion DNA polymerase (New England BioLabs, M0530) with 31 µl water. PCR was performed according to the manufacturer's instructions. PCR samples were purified using a QIAquick PCR purification kit (Qiagen, 28104) and eluted with 30 °C water. 16S rDNA PCR product was cloned using a ZeroBlunt TOPO PCR Cloning kit (Thermo Fisher Scientific, K280020) according to the manufacturer's instructions and Sanger sequenced at the Harvard Biopolymers Facility using the M13 forward (5'-GTAAAACGACGGCCAG-3') or M13 reverse (5'-CAGGAACAGCTATGAC-3') primers. Individual sequences were identified using NCBI BlastN. Species were identified by having >99% identity to published sequences.

On the first dilution plate in which individual colonies could be observed, we isolated and sequenced 24 different colonies and identified seven different species of bacteria, five Gram-positive anaerobes (*Blautia hydrogenotrophica*, *Clostridium orbiscindens*, *Clostridium innocuum*, *C. cateniformis* and *E. ramosum*), one facultative Gram-positive (*Longicatena caecimuris*) and one Gram-negative anaerobe (*Phocaeicola dorei*). The combination of these seven different species promoted an anti-tumour response to anti-PD-L1 therapy in GF mice (Extended Data Fig. 6a). From these seven, we next tested the combination of the three Gram-positive anaerobes that have been reported as human commensal bacteria (*C. innocuum*, *C. cateniformis*, *E. ramosum*) and found that this combination was also sufficient to promote an anti-tumour response in GF mice (Extended Data Fig. 6b). We further monocolonized mice with each of these bacteria and found that colonization with either *C. cateniformis* or *E. ramosum* was sufficient to promote anti-tumour immunity to anti-PD-L1 (Fig. 2f and Extended Data Fig. 6c,d), whereas colonization with *C. innocuum* did not (Extended Data Fig. 6e).

Bacterial DNA isolation for quantitative PCR

C. cateniformis, *E. ramosum* and HMB stocks were pelleted, and pellets and Taconic stool samples were extracted by phenol–chloroform extraction as previously described³¹. Reactions comprised 50 ng of extracted DNA as template, 10 µl SSoAdvanced Universal SYBRGreen Super Mix (Bio-Rad, 175270), 10 µl PCR-grade water and 0.25 µl of forward and reverse primers at 10 µM and analysed on a QuantStudio5

instrument. The following primers were used: universal forward, 5'-CTCCTACGGGAGGCAGCAG-3'; universal reverse, 5'-TTACCGCGG CTGCTGGCAC-3'; *C. cateniformis*-F, 5'-ACCGCATAGGTGAAGGGGTC-3'; and *C. cateniformis*-R, 5'-GAATCATTTCTATTTCATA-3' (ref. 17). Cycle conditions were 95 °C for 3 min followed by 39 cycles (95 °C for 10 s, 55 °C for 30 s, 95 °C for 10 s, 65 °C for 5 s and 95 °C for 5 s). For each sample, *C. cateniformis* Ct values were normalized to universal 16S Ct values.

Preparation of bacteria

C. cateniformis, *E. ramosum* and *C. innocuum* stocks were plated on Brucella plates and stored in an anaerobic chamber for 3 days. Individual colonies were inoculated in chopped meat medium (Anaerobe Systems, AS-811). The OD₆₀₀ was measured, and 200 µl of overnight culture was orally gavaged into GF mice in isolators 1 week before tumour implantation.

For *C. cateniformis* bacterial extracts, individual colonies were inoculated in reinforced clostridia medium overnight in an anaerobic chamber. Next 1 ml of overnight culture was used to inoculate 10 litres of reinforced clostridia medium and the culture was left to grow for 2–3 days. Surface extracts were isolated as previously described³⁴.

Cell lines

MC38 and B16-OVA³⁵ cells were cultured in DMEM supplemented with 10% FBS and 1% penicillin–streptomycin at 37 °C in the presence of 5% CO₂. B16-OVA cells were selected for 2 days with 2 µg ml⁻¹ puromycin after thawing a new batch of cells. E0771 (American Type Culture Collection (ATCC), CRL3461), LLC (ATCC, CRL1642) and MB49 (Sigma, SCC148) were cultured in DMEM supplemented with 10% FBS and 1% penicillin–streptomycin at 37 °C in the presence of 5% CO₂. PY8119 (ATCC, CRL3278) was cultured in F12 medium supplemented with 5% FBS and 1% penicillin–streptomycin at 37 °C in the presence of 5% CO₂. To create OVA-expressing cell lines of LLC and PY8119, lentivirus was produced by transfecting 293× cells with the packaging plasmids pMD2.G (Addgene, 12259) and psPAX2 (Addgene, 12260), and the OVA expression plasmid (pLX305-BlastR-OVA). LLC and PY8119 cells were transduced with lentiviral supernatants and polybrene as a transduction enhancer. Transduced cells were then selected with blasticidin and confirmed to express the SIINFEKL peptide by flow cytometry following stimulation with IFNγ. All cell lines were confirmed to be mycoplasma negative.

BMDC generation

Bone marrow cells were isolated from mouse femurs and cultured in RPMI 1640 medium supplemented with 10% FBS, 1% penicillin–streptomycin, 10 mM HEPES, 1 mM sodium pyruvate, 55 µM β-mercaptoethanol and 20 ng ml⁻¹ of GM-CSF (R&D Systems, 315-03) and 20 ng ml⁻¹ of IL-4 (BioLegend, 574302) for BMDCs at 37 °C in the presence of 5% CO₂. GM-CSF and IL-4 were refreshed every 2 days.

In vitro CD8⁺ T cell differentiation and proliferation assay

Naive CD8⁺ T cells were purified from splenocytes of OT-1 (C57BL/6-Tg(TcrαTcrβ)1100Mjb/J) *Rgmb*^{fl/fl} and OT-1 *Rgmb*^{fl/fl} CD4-Cre⁺ mice using a Naive CD8⁺ T cell isolation kit (Miltenyi Biotec, 130-093-543). The purified naive CD8⁺ T cells were labelled with 5 µM Cell Trace Violet Proliferation dye (Thermo Fisher Scientific, C34557) and cultured with BMDCs at a ratio of 5:1 in the presence of 100 U ml⁻¹ of IL-2 (PeproTech, 200-02) and OVA(257–264) peptide (Anaspec, AS-60193-1) for 72 h. For measurement of cytokine production, the cells were re-stimulated with Golgi inhibitors and PMA and ionomycin for 5 h, followed by intracellular cytokine staining.

Tumour-infiltrating leukocyte isolation

Tumours were collected at days 10–16 after implantation, mechanically dissociated and incubated in DPBS containing calcium, magnesium and 250 U ml⁻¹ of type 1 collagenase (Worthington Biochemical) for 20 min

Article

at 37 °C with gentle rocking. After filtration, tumour-infiltrating lymphocytes were isolated by Percoll density gradient (40%/70%) centrifugation at 800g for 20 min without brake. The interface of the Percoll layers were recovered for further analyses.

Flow cytometry and cell sorting

Primary mouse cells were isolated from dLNs, MLNs and tumours. Single-cell suspensions were prepared with a 70 µm cell strainer and incubated with TruStain FcX (BioLegend, 101319) to block Fc receptors before staining. Cells were stained using a Live/Dead Fixable Near-IR Dead Cell Stain kit (Thermo Fisher Scientific, L34975) according to the manufacturer's instructions. Surface antigen staining was performed in DPBS containing 1% FBS and 2 mM EDTA, followed by intracellular staining using an eBioscience FXP3/Transcription Factor Staining Buffer Set (Thermo Fisher Scientific, 00-5523-00). For intracellular cytokine staining, isolated cells were stimulated with 50 ng ml⁻¹ of phorbol 12-myristate 13-acetate and 500 ng ml⁻¹ of ionomycin for 5 h in the presence of 1× GolgiPlug protein transport inhibitor (BD Biosciences, 555029) and 1× GolgiStop protein transport inhibitor (BD Biosciences, 554724) before intracellular staining. The following antibodies were used for staining procedures: BUV395 anti-mouse CD8β clone H35-17.2 (BD Biosciences, 740278; 1:200); Brilliant Violet 421 anti-mouse CD8β clone YTS156.7.7 (BioLegend, 126629; 1:200); PerCP-Cy5.5 anti-mouse CD8β clone YTS156.7.7 (BioLegend, 126610; 1:200); Alexa Fluor 700 anti-mouse CD8α clone 53-6.7 (BioLegend, 100730; 1:200); BUV395 anti-mouse I-A/I-E clone 2G9 (BD Biosciences, 743876; 1:500); Pacific Blue anti-mouse I-A/I-E clone M5/114.15.2 (BioLegend, 107620; 1:500); BUV737 anti-mouse CD45.2 clone 104 (BD Biosciences, 564880; 1:200); Brilliant Violet 711 anti-mouse CD44 clone IM7 (BioLegend, 103057; 1:200); Brilliant Violet 605 anti-mouse CD44 clone IM7 (BioLegend, 103047; 1:200); Alexa Fluor 700 anti-mouse CD45 clone 30-F11 (BioLegend, 103128; 1:200); Brilliant Violet 510 anti-mouse CD45 clone 30-F11 (BioLegend, 103138; 1:200); PE-Texas Red anti-mouse CD4 clone RM4-5 (Thermo Fisher Scientific, MCD0417; 1:200); BUV564 anti-mouse CD4 clone GK1.5 (BD Biosciences, 612923; 1:200); PE anti-mouse CD4 clone GK1.5 (BioLegend, 100408; 1:200); PE-Cy7 anti-mouse IL-17A clone TC11-18H10.1 (BioLegend, 506922; 1:200); Brilliant Violet 510 anti-mouse CD366 clone 5D12/TIM-3 (BD Biosciences, 747625; 1:200); Brilliant Violet 711 anti-mouse CD366 clone 7D3 (BD Biosciences, 565566; 1:200); PE-CF594 anti-mouse CD11b clone M1/70 (BD Biosciences, 562317; 1:200); BUV805 anti-mouse CD11b clone M1/70 (BD Biosciences, 741934; 1:200); Brilliant Violet 605 anti-mouse CD11b clone M1/70 (BD Biosciences, 563015; 1:200); BUV496 anti-mouse CD3ε clone 145-2C11 (BD Biosciences, 564661; 1:200); Brilliant Violet 570 anti-mouse CD3ε clone 17A2 (BioLegend, 100225; 1:200); PE-Cy7 anti-mouse CD3ε clone 17A2 (BioLegend, 100220; 1:200); Brilliant Violet 570 anti-mouse TCRβ clone H57-597 (BioLegend, 109231; 1:200); BUV615 anti-mouse TCRβ clone H57-597 (BD Biosciences, 751212; 1:200); APC anti-mouse IFNγ clone XMG1.2 (BioLegend, 505810; 1:200); PerCP-eFluor 710 anti-mouse CD274 clone MH5 (Thermo Fisher Scientific, 46-5982-82; 1:200); BUV737 anti-mouse CD80 clone 16-10A1 (BD Biosciences, 564670; 1:200); PE-Cy7 anti-mouse CD11c clone HL3 (BD Biosciences, 558079; 1:200); Brilliant Violet 510 anti-mouse CD11c clone HL3 (BD Biosciences, 562949; 1:200); FITC anti-mouse CD11c clone N418 (BioLegend, 117306; 1:200); PE anti-mouse CD11c clone N418 (BioLegend, 117307; 1:200); PerCP-Cy5.5 anti-mouse TNF-α clone MP6-XT22 (BioLegend, 506322; 1:200); Brilliant Violet 711 anti-mouse TNF-α clone MP6-XT22 (BioLegend, 506349; 1:200); FITC anti-human/mouse granzyme B clone GB11 (BioLegend, 515403; 1:200); PE-Cy7 anti-human/mouse granzyme B clone QA16A02 (BioLegend, 372214; 1:200); Brilliant Violet 605 anti-mouse CD279 clone 29F.1A12 (BioLegend, 135220; 1:200); PE-Cy7 anti-mouse galectin-9 clone RG9-35 (BioLegend, 136113; 1:200); Brilliant Violet 510 anti-mouse CD40 clone 3/23 (BD Biosciences, 745041; 1:200); PerCP-Cy5.5 anti-human/mouse/rat CD278 clone C398.4A (BioLegend, 313518; 1:200); PE-Cy7 anti-mouse CD252 clone

RM134L (BioLegend, 108813; 1:200); biotinylated anti-mouse RGMb polyclonal antibody (R&D Systems, BAF3597; 1:200); APC streptavidin (BioLegend, 405243; 1:200); Brilliant Violet 605 anti-mouse CD86 clone GL1 (BD Biosciences, 563055; 1:200); PE anti-mouse CD275 (BioLegend, 107405; 1:200); Brilliant Violet 421 anti-mouse CD273 clone TY25 (BioLegend, 107219; 1:200); APC anti-mouse CD273 clone TY25 (BioLegend, 107210; 1:200); PE anti-mouse CD223 clone eBioC9B7W (Thermo Fisher Scientific, 12-2231-82; 1:200); PE-Cy7 T-bet clone 4B10 (BioLegend, 644823; 1:200); PE anti-mouse CD107a clone 1D4B (BioLegend, 121612; 1:200); and BV711 anti-mouse IL-2 clone JES6-5H4 (BioLegend, 503837; 1:200). Alexa Fluor 594 anti-RGMb clone 9D3 antibody (1:100) was generated in G. Freeman's laboratory as previously described²⁷. Flow cytometry analyses were performed on a BD LSR II or BD FACSymphony. For cell sorting, a BD FACS Aria II was used. Data were collected using BD DIVA 9 software analysed using FlowJo (v.10.8.1) software. Gating strategies are displayed in Extended Data Fig. 10.

Quantitative real-time PCR analysis

Cells were sorted using a FACS BD Aria II and lysed with RLT lysis buffer. RNA was extracted using a Qiagen RNeasy Plus Mini kit (Qiagen, 74236). cDNA was generated using a SuperScript VIL0 cDNA synthesis kit (Thermo Fisher Scientific, 11754250) and analysed on a LightCycler 96 machine and LightCycler 96 1.1 software using Applied Biosystems TaqMan Fast Advanced master mix (Fisher Scientific, 44-445-57) and Taqman probes (ThermoFisher Scientific, 4331182 and 4319413E).

Lentiviral production

Lentiviruses were generated using a LV-MAX lentiviral production system (Thermo Fisher, A35684). In brief, HEK293F cells were transfected with a mixture of pLV-C-GFPspark lentiviral vector (Sino Biological) or pLV-mPD-L2-GFPspark lentiviral vector and LV-MAX lentiviral packaging mix (Thermo Fisher, A43237) using a LV-MAX transfection reagent kit (Thermo Fisher, 35348) following the manufacturer's instruction. The supernatants from the cell culture were obtained and concentrated using Lenti-X concentrator (Takara, 631232).

Adoptive transfer of BMDCs

WT or *Pd12* KO bone marrow cells were cultured in the presence of 20 ng ml⁻¹ of GM-CSF for 6 days to generate BMDCs, followed by pulsing with 100 µg ml⁻¹ of OVA protein (Endofit, vac-pova) for 24 h in the presence of 10 µg ml⁻¹ of *C. cateniformis* extract or vehicle control. On day 3 after implantation, 5 × 10⁵ of OVA-pulsed BMDCs were subcutaneously injected into B16-OVA-tumour bearing mice at the tumour site³⁶. For PD-L2-overexpressing BMDCs, the cells were infected with lentivirus at a multiplicity of infection of 30 by spin-inoculation for 90 min at 25 °C in the presence of 8 µg ml⁻¹ of polybrene (Millipore Sigma, TR-1003G) on BMDC culture days 3 and 4. On day 7, GFP-expressing BMDCs were sorted by FACS, followed by subsequent culture for 2 days in the presence of 20 ng ml⁻¹ of GM-CSF. GFP-expressing BMDCs were pulsed with OVA protein for 24 h, and 2 × 10⁵ cells were subcutaneously injected into the B16-OVA tumour site on day 3 after implantation.

Statistical analysis

Statistical analyses were performed using GraphPad Prism 9 software. Statistical significance was determined as *P* < 0.05 using unpaired Student's *t*-test for comparing two groups or nonparametric one-way analysis of variance (ANOVA) for comparisons with more than two groups. Two-way ANOVA was used for tumour growth curves with multiple groups, followed by Bonferroni's, Tukey's or Sidak's multiple comparison test as indicated. All the data are presented as the mean ± s.e.m. or s.d. *P* values are denoted in figures, where NS is not significant.

Reporting summary

Further information on research design is available in the Nature Portfolio Reporting Summary linked to this article.

Data availability

The 16S sequencing data have been deposited to National Institutes of Health BioProject database with the identifier PRJNA936792. Source data are provided with this paper.

29. Lo, M. et al. Effector-attenuating substitutions that maintain antibody stability and reduce toxicity in mice. *J. Biol. Chem.* **292**, 3900–3908 (2017).
30. Eisenhauer, E. A. et al. New response evaluation criteria in solid tumours: revised RECIST guideline (version 1.1). *Eur. J. Cancer* **45**, 228–247 (2009).
31. Wu, M. et al. Genetic determinants of in vivo fitness and diet responsiveness in multiple human gut *Bacteroides*. *Science* **350**, aac5992 (2015).
32. Caporaso, J. G. et al. Ultra-high-throughput microbial community analysis on the Illumina HiSeq and MiSeq platforms. *ISME J.* **6**, 1621–1624 (2012).
33. Bolyen, E. et al. Reproducible, interactive, scalable and extensible microbiome data science using QIIME 2. *Nat. Biotechnol.* **37**, 852–857 (2019).
34. Deng, L., Kasper, D. L., Krick, T. P. & Wessels, M. R. Characterization of the linkage between the type III capsular polysaccharide and the bacterial cell wall of group B *Streptococcus*. *J. Biol. Chem.* **275**, 7497–7504 (2000).
35. LaFleur, M. W. et al. PTPN2 regulates the generation of exhausted CD8⁺ T cell subpopulations and restrains tumor immunity. *Nat. Immunol.* **20**, 1335–1347 (2019).
36. Dixon, K. O. et al. TIM-3 restrains anti-tumour immunity by regulating inflammasome activation. *Nature* **595**, 101–106 (2021).

Acknowledgements Figure 4a was created using BioRender (<https://www.biorender.com>). We would like to thank T. Yanortsang and J. Ramos for their assistance with GF mice; and members of the Sharpe Laboratory and the Kasper Laboratory for insightful discussions. The following institutions are acknowledged for funding: Quark Ventures (A31696 to J.S.P., F.S.G., D.L.K. and A.H.S.); the National Institutes of Health/National Institute of Childhood Health and Human Disease (T32 5T32HD55148-10 to F.S.G.); the National Institutes of Health/National Cancer Institute (1 K22 CA258960-01 to F.S.G.; 5F32CA247072-02 to J.S.P.; P50CA206963 and P50CA101942 to G.J.F.; P01 AI56299 to A.H.S. and G.J.F.; and 1F32CA260769-01 to G.M.); and the Cancer Prevention and Research Institute of Texas (CPRIT Training Award RP210028 to E.M.P.).

Author contributions J.S.P., F.S.G., G.J.F., D.L.K. and A.H.S. designed the experiments. J.S.P. and F.S.G. performed the experiments. M.W. analysed the 16S sequencing data. A.K.L., J.G., M.W.L. and W.Z. assisted with the experiments. S.B.J., G.M., E.M.P., Y.Z., S.S.W. and J.A.W. obtained the patient stool samples. J.S.P. and F.S.G. analysed the data. G.J.F. generated the PD-L1, PD-L2 and RGMb antibodies. J.S.P., F.S.G., G.J.F., D.L.K. and A.H.S. wrote the manuscript.

Competing interests J.S.P., F.S.G., D.L.K. and A.H.S. are listed as inventors on US Utility application (17/311,587) covering identification of gut bacteria that promote an anti-tumour response to immunotherapy filed by President and Fellows of Harvard College. J.S.P., F.S.G., D.L.K. and A.H.S. are listed as inventors on US Utility application (17/473,083) covering methods

and compositions for treating cancer or a tumour in a subject by administering to the subject a first agent that disrupts the interaction between PDL2/RGMb and a second agent that disrupts the interaction between PD-1/PD-L1 filed by President and Fellows of Harvard College. J.S.P., F.S.G., G.J.F., D.L.K. and A.H.S. are listed as inventors on PCT patent applications (PCT/US21/50674) covering methods of treating an individual that has failed an anti-PD-1/PD-L1 therapy filed by President and Fellows of Harvard College and Dana-Farber Cancer Institute. J.S.P., F.S.G., G.J.F., D.L.K. and A.H.S. are listed as inventors on PCT patent applications (PCT/US23/12139) covering methods and compositions for treating cancer or a tumour in a subject by administering to the subject T cells with reduced RGMb expression or activity and an immune checkpoint inhibitor such as a PD-1 or PD-L1 inhibitor filed by President and Fellows of Harvard College and Dana-Farber Cancer Institute. J.S.P., F.S.G., G.J.F., D.L.K. and A.H.S. are listed as inventors on provisional patent application covering PD-L2 modulated dendritic cell therapy filed by President and Fellows of Harvard College and Dana-Farber Cancer Institute. G.J.F. is listed as an inventor on US patent US11220545 on combination RGMb and PD-1 blockade for cancer immunotherapy assigned to Dana-Farber Cancer Institute. G.J.F. and A.H.S. have patents/pending royalties on the PD-1–PD-L1 pathway from Roche, Merck MSD, Bristol-Myers Squibb, Merck KGA, Boehringer-Ingelheim, AstraZeneca, Dako, Leica, Mayo Clinic, and Novartis as listed in Supplementary Table 1. G.J.F. has served on advisory boards for Roche, Bristol-Myers-Squibb, Xios, Origimed, Triursus, iTeos, NextPoint, IgM, Jubilant, Trillium, GV20, IOME, and Geode. G.J.F. has equity in Nextpoint, Triursus, Xios, iTeos, IgM, Trillium, Invaria, GV20, and Geode. A.H.S. has patents/pending royalties on the PD-1 pathway from Roche and Novartis. A.H.S. is on advisory boards for Surface Oncology, SQZ Biotechnologies, Elpiscience, Selecta, Bicara and Monopteros, Bicara, Fibrogen, IOME and Alixia. She also is on scientific advisory boards for the Massachusetts General Cancer Center, Program in Cellular and Molecular Medicine at Boston Children’s Hospital, the Human Oncology and Pathogenesis Program at Memorial Sloan Kettering Cancer Center, Bloomberg-Kimmel Institute for Cancer Immunotherapy, GlaxoSmithKline, Janssen and Amgen. She is an academic editor for the *Journal of Experimental Medicine*. A.H.S. has received research funding from Novartis, Roche, UCB, Ipsen, Merck, AbbVie, Moderna, Vertex and Erasca unrelated to this project. D.L.K. is on a scientific advisory board of IOME. S.S.W. is on the advisory board for Asyilia Therapeutics and reports compensation from Ridgeline Therapeutics. J.A.W. reports compensation for speaker’s bureau and honoraria from Imedex, Dava Oncology, Omniprex, Illumina, Gilead, PeerView, Physician Education Resource, MedImmune, and Bristol-Myers Squibb and serves as a consultant and advisory board member for Roche/Genentech, Novartis, AstraZeneca, GlaxoSmithKline, Bristol-Myers Squibb, Merck, Micronoma, and Biothera Pharmaceuticals, with stock options for Micronoma.

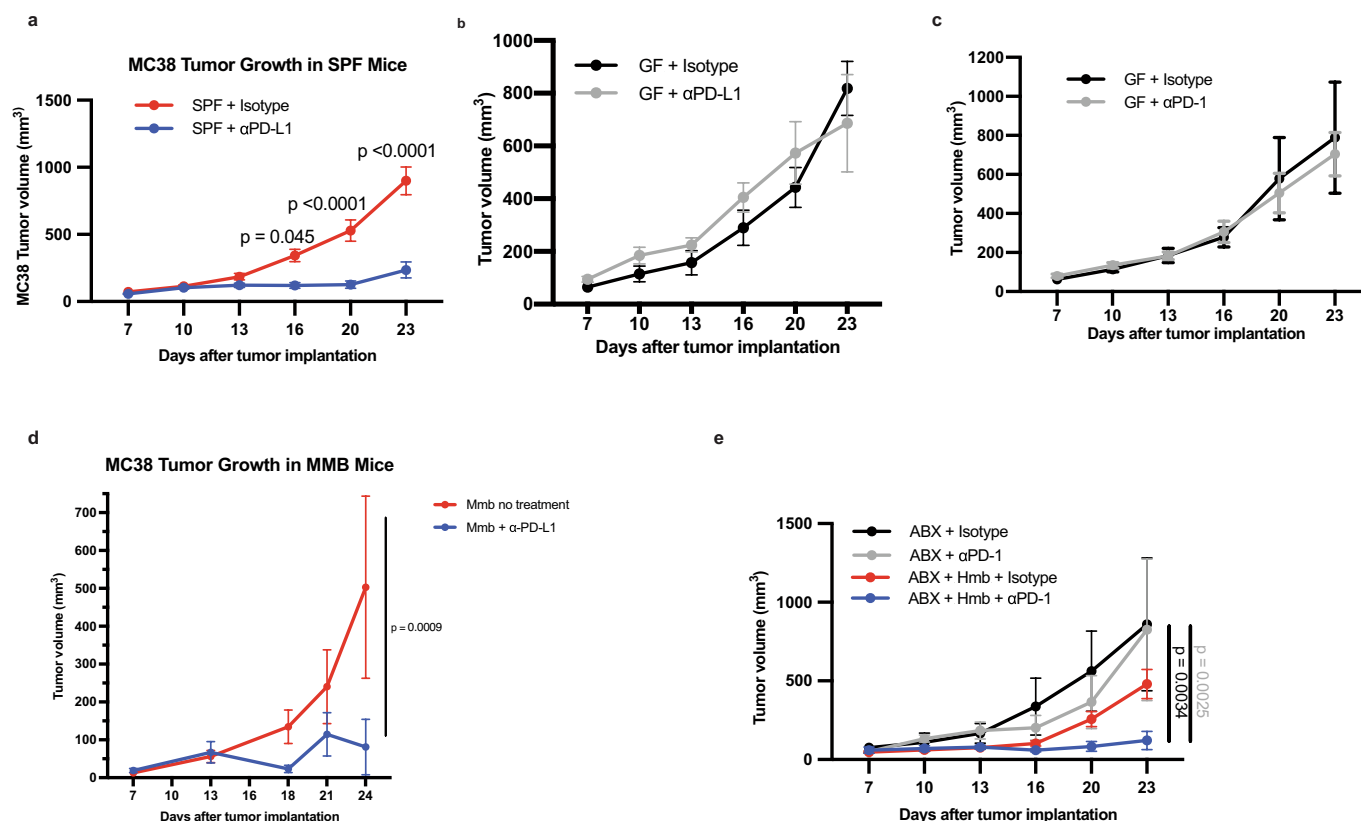
Additional information

Supplementary information The online version contains supplementary material available at <https://doi.org/10.1038/s41586-023-06026-3>.

Correspondence and requests for materials should be addressed to Gordon J. Freeman, Dennis L. Kasper or Arlene H. Sharpe.

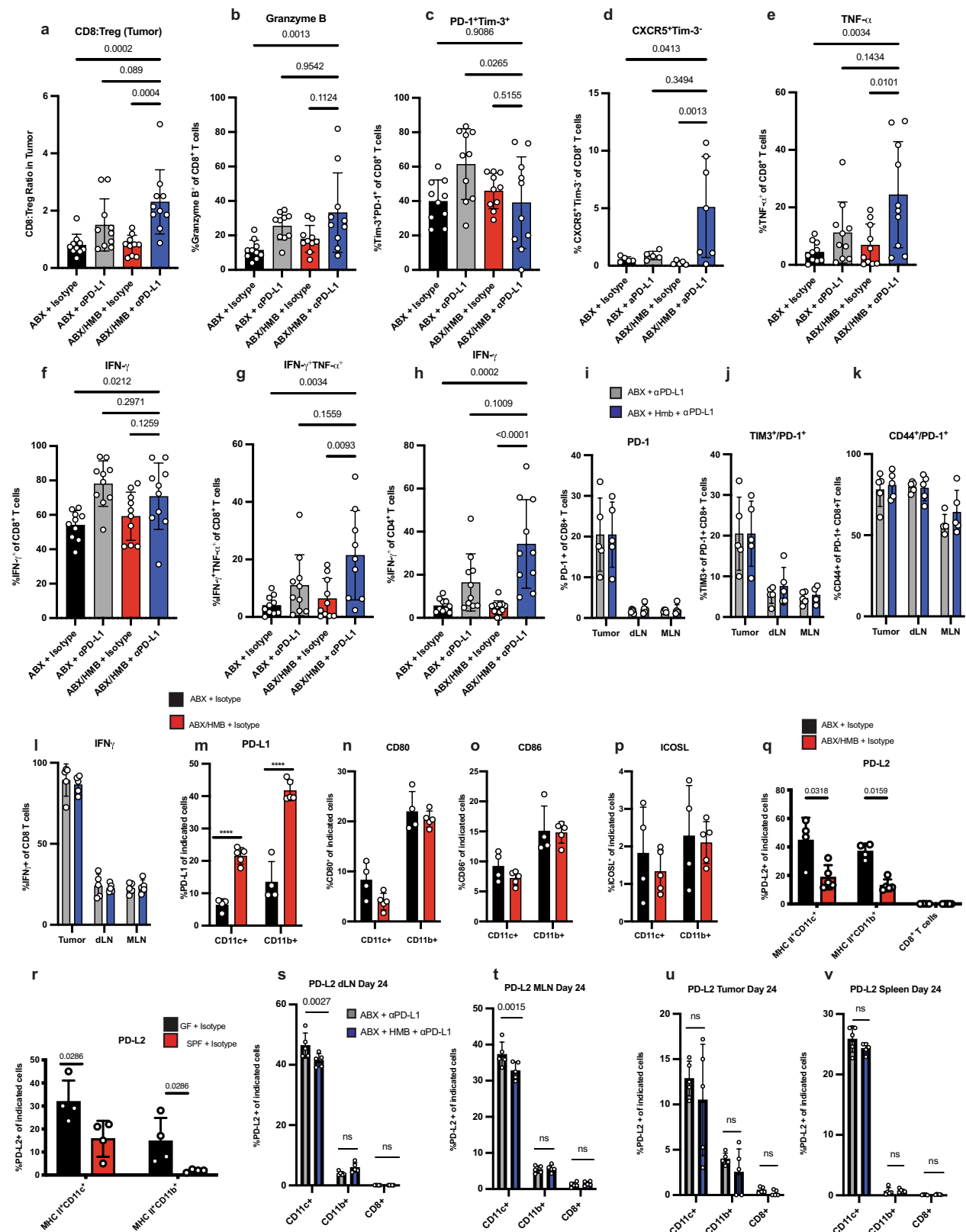
Peer review information *Nature* thanks the anonymous reviewers for their contribution to the peer review of this work.

Reprints and permissions information is available at <http://www.nature.com/reprints>.



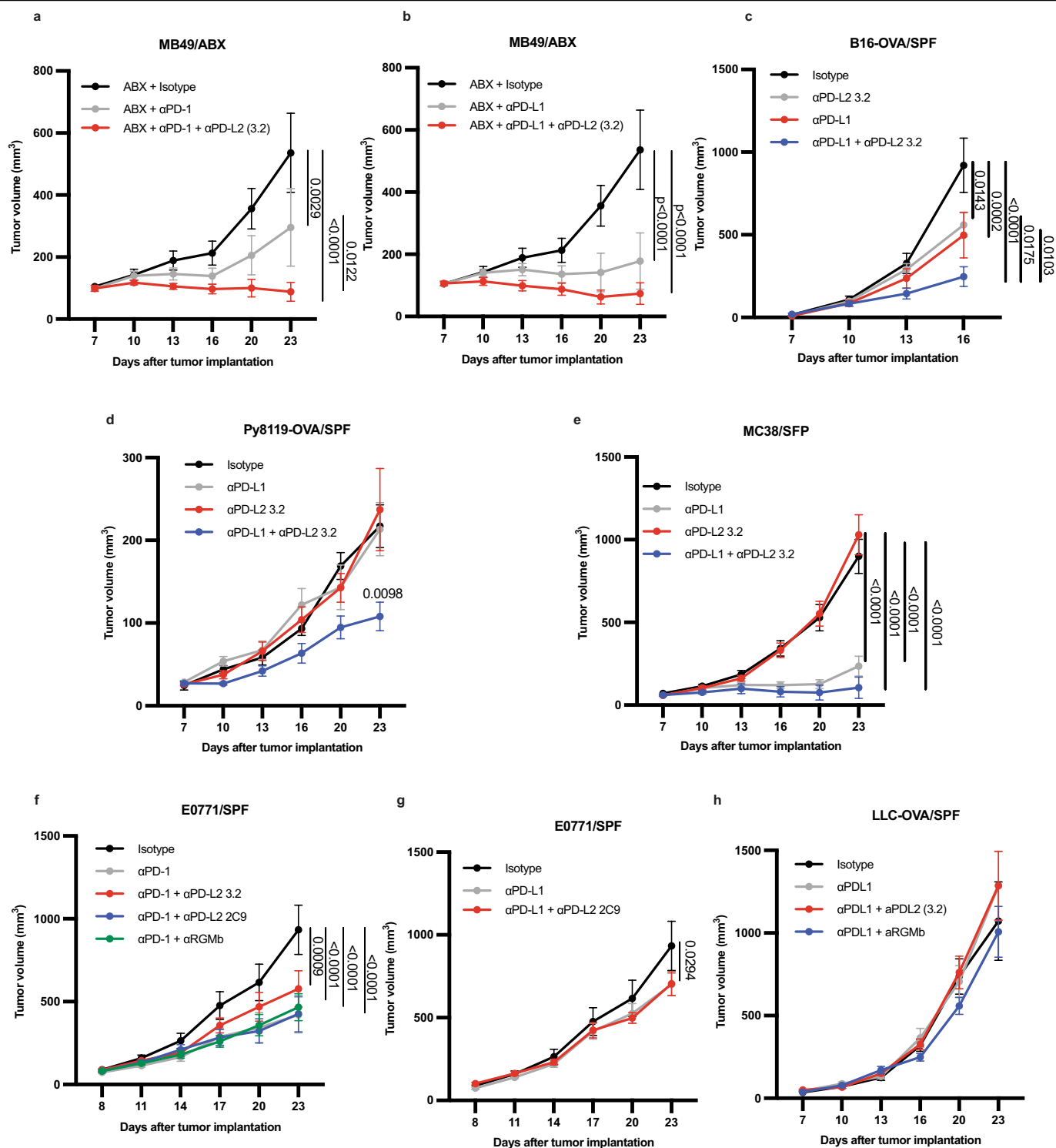
Extended Data Fig. 1 | SPF, MMB, and HMB promote anti-tumor responses to PD-1/PD-L1 blockade. MC38 tumor growth with or without anti-PD-L1 in (a) Taconic SPF $n = 10$ mice per group. Significance indicated on graph and measured by Two Way ANOVA and Sidak's multiple comparisons test or (b) GF $n = 5$ mice per group, performed at the same time as (a), representative experiment of 14 individual experiments. MC38 tumor cells were implanted subcutaneously in (c) GF mice $n = 4$ mice for isotype group and $n = 5$ mice for anti-PD-1 group. (d) GF mice were orally gavaged with MMB one week before implantation of MC38 tumor cells. $N = 3$ mice for no treatment group and $n = 6$

mice for anti-PD-L1 group. Significance indicated on graph and measured by Two Way ANOVA and Sidak's multiple comparisons test. (e) MC38 tumor cells were implanted subcutaneously in ABX or ABX/HMB mice and treated with anti-PD-1 according to Fig. 1a, and monitored for tumor growth. $N = 3$ mice for ABX + isotype group and $n = 4$ mice for ABX + anti-PD-1, ABX/HMB + Isotype, and ABX/HMB + anti-PD-1 groups. Significance indicated on graph and measured by Two-Way ANOVA and Tukey's multiple comparisons test. (a-e) Error bars show mean and s.e.m.



Extended Data Fig. 2 | Immune cell responses in ABX, ABX/HMB, GF, and SPF mice. MC38 tumor cells were implanted subcutaneously in ABX and ABX/HMB mice. Mice were treated with isotype or anti-PD-L1 on days 7, 10, 13, and 16, followed by sacrificed on day 24 after tumor implantation. For detection of cytokines, tumor-infiltrating lymphocytes were stimulated with PMA/Ionomycin for 5 h in the presence of Golgi inhibitors. (a) Ratio of CD8⁺ T cells to Treg cells n = 10 mice per group (b) Percent of Granzyme B⁺ CD8⁺ T cells n = 10 mice per group (c) Frequency of PD-1⁺ TIM-3⁺ n = 10 mice per group or (d) CXCR5⁺ TIM-3⁺ among CD8⁺ T cells in tumors n = 5 mice per group for ABX groups and ABX/HMB+ Isotype group and n = 7 for ABX/HMB + anti-PD-L1 group. Percent of (e) TNF- α ⁺ n = 10 mice per group (f) IFN γ ⁺ n = 10 mice per group, and (g) TNF- α ⁺ IFN γ ⁺ CD8⁺ T cells n = 10 mice per group for ABX groups and ABX/HMB + isotype and n = 9 mice for ABX/HMB + anti-PD-L1 (h) Percent of IFN γ ⁺ CD4⁺ T cells n = 10 mice per group for ABX groups and ABX/HMB + anti-PD-L1 and n = 12 mice per group for ABX/HMB + isotype. Mice were analyzed on day 24 after tumor implantation, representative of two independent experiments. Significance measured by non-parametric one-way ANOVA and Dunn's multiple comparisons and P values are indicated on graphs, error bars show mean and s.d. (i-l) MC38 tumor cells were implanted subcutaneously in ABX and ABX/HMB mice. Mice were treated with isotype or anti-PD-L1 on days 7 and 10 and sacrificed on day 13 after tumor implantation. (i) Percent of PD-1⁺ CD8⁺ T cells in tumors, dLNs, and mesenteric lymph nodes (MLNs) n = 5 mice per group (j) Percent TIM-3⁺ among PD-1⁺ CD8⁺ T cells in Tumors, dLNs, and MLNs n = 5 mice per group for all except MLN ABX/HMB + anti-PD-L1 n = 4 mice

per group (k) Percent CD44⁺ expression on PD-1⁺ CD8⁺ T cells in tumors, dLNs, and MLNs n = 4 mice per group (l) Percent IFN γ ⁺ CD8⁺ T cells in tumors, dLNs, and MLNs n = 5 mice per group. (i-l) Significance determined by non-parametric one-way ANOVA with Dunn's multiple comparisons test, error bars show mean and s.d. Expression of (m) PD-L1, (n) CD80, (o) CD86, and (p) ICOSL on CD11c⁺ MHCII⁺ and CD11b⁺ MHCII⁺ cells in draining lymph nodes of ABX and ABX/HMB mice implanted with MC38 tumor cells subcutaneously and treated with isotype control mAb as in Fig. 1a. Mice were analyzed on day 13 after tumor implantation. N = 4 mice in ABX group and n = 5 mice in ABX/HMB group. Significance measured by unpaired two-tailed, Mann-Whitney test. Expression of PD-L2 on CD11c⁺ MHCII⁺, CD11b⁺ MHCII⁺ cells and CD8⁺ T cells in draining lymph nodes of (q) ABX vs. ABX/HMB mice n = 4 mice per group for ABX and n = 5 mice per group for ABX/HMB or (r) GF vs. Taconic SPF mice n = 4 mice per group, implanted with MC38 tumor cells subcutaneously and treated with isotype control mAb as in Fig. 1a. Mice were analyzed on day 10 after tumor implantation. Significance measured by unpaired, two-tailed Mann-Whitney test, and significant P values indicated on graphs. ABX and ABX/HMB mice were sacrificed 24 days after implantation with MC38 tumor cells. PD-L2 was measured on MHCII⁺ CD11c⁺, MHCII⁺ CD11b⁺, and CD8⁺ T-cells in (s) draining lymph nodes n = 5 mice per group, (t) MLN n = 5 mice for ABX and n = 4 mice for ABX/HMB, (u) tumors n = 5 mice per group and (v) spleen n = 5 mice per group. Significance measured by Two-Way ANOVA and Sidak's multiple comparison's test. Significant P values indicated on graph. Representative experiment of two different experiments. Error bars show mean and s.d.



Extended Data Fig. 3 | See next page for caption.

Extended Data Fig. 3 | Combination therapy with anti-PD-1 or anti-PD-L1 plus anti-PD-L2 or anti-RGMb promotes an anti-tumor response in multiple, but not all, tumor types in SPF mice. MC38, B16-OVA, MB49, Py8119-OVA, LLC-OVA cells were implanted subcutaneously, and E0771 cells were injected into mammary fat pad of C57BL/6 mice with the indicated microbiota. The mice were treated with four doses of anti-PD-L1 or anti-PD-1 with/without anti-PD-L2 3.2 or anti-PD-L2 2C9 or anti-RGMb 9D1 one week after tumor implantation as indicated. **(a)** Growth of MB49 tumors in ABX mice given isotype, anti-PD-1 alone or combined with anti-PD-L2 3.2 n = 10 mice per group for Isotype and anti-PD-1 + anti PD-L2 3.2 groups, n = 9 mice for anti-PD-1 group **(b)** Growth of MB49 tumors in ABX mice given isotype, anti-PD-L1 alone or combined anti-PD-L2 3.2 n = 10 mice per group **(c)** Growth of B16-OVA tumors in Taconic SPF mice given isotype, anti-PD-L1, anti-PD-L2 3.2 or anti-PD-L1 + anti-PD-L2. n = 5 mice per group for isotype and anti-PD-L2 3.2 groups and n = 10

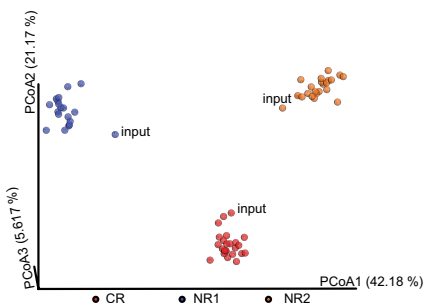
mice per group for anti-PD-L1 and anti-PD-L1 + anti-PD-L2 3.2 groups. **(d)** Growth of Py8119-OVA in Taconic SPF mice given isotype or anti-PD-L1 and/or anti-PD-L2 3.2. n = 5 mice per group for all except n = 4 mice for anti-PD-L2 3.2 group **(e)** Growth of MC38 tumors in Taconic SPF mice given isotype, anti-PD-L1, anti-PD-L2 3.2, or anti-PD-L1 + anti-PD-L2 n = 10 mice per group for all except n = 9 mice for anti-PD-L2 3.2 group. **(f-g)** Growth of E0771 tumors in Taconic SPF mice **(f)** given isotype, or anti-PD-1 combined with anti-PD-L2 3.2, anti-PD-L2 2C9 or anti-RGMb 9D1 n = 10 mice per group or **(g)** given isotype n = 10 mice, anti-PD-L1 alone n = 9 mice or combined with anti-PD-L2 n = 5 mice. **(h)** Growth of LLC-OVA tumors in Taconic SPF mice given isotype, anti-PD-L1, or anti-PD-L1 and either anti-PD-L2 3.2 or anti-RGMb 9D1. n = 10 mice per group. Significance measured by two-way ANOVA and Tukey's multiple comparisons test. Significant P values are designated on graphs. Error bars show mean and s.e.m.

a

Patient characteristics for stool samples

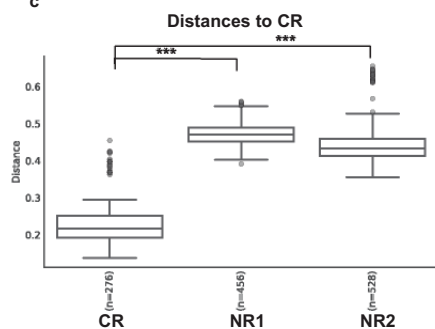
Sample	Age	Sex	Stage	BMI	ICB	Other Tx	Fecal Sample Collection Timepoint
CR	62	M	IV M1b	27.09	Pembrolizumab	None	Post-ICB (2yr post-treatment)
NR1	50	F	IIIB	42.31	Pembrolizumab	INCB001158	During ICB (1yr post-start)
NR2	57	F	IIIC	20.4	Nivolumab	None	During ICB (3mo post-start)

b

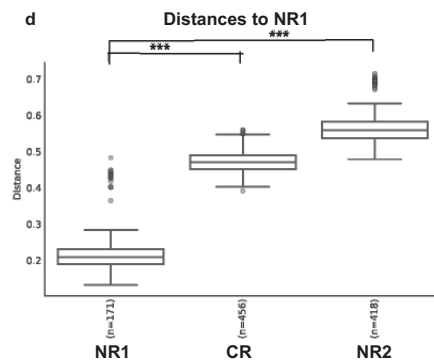


Unweighted

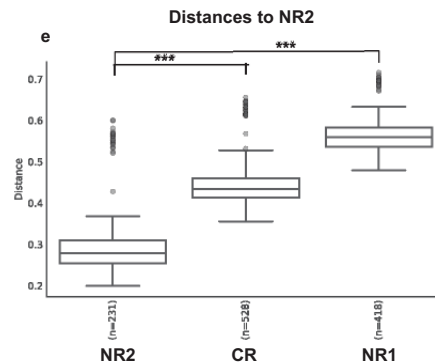
c



d

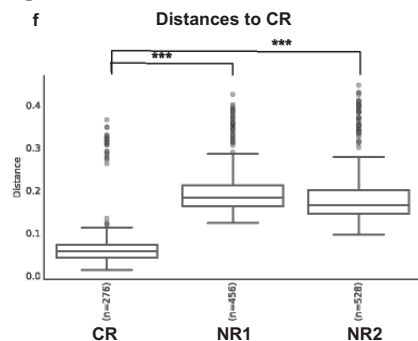


e

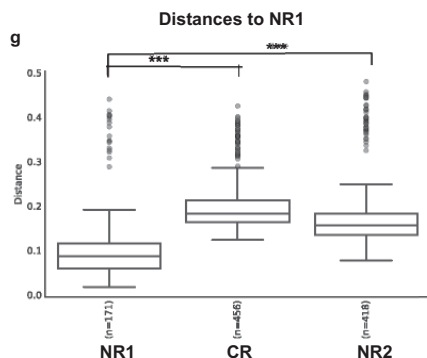


Weighted

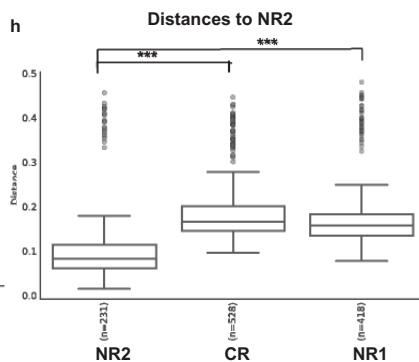
f



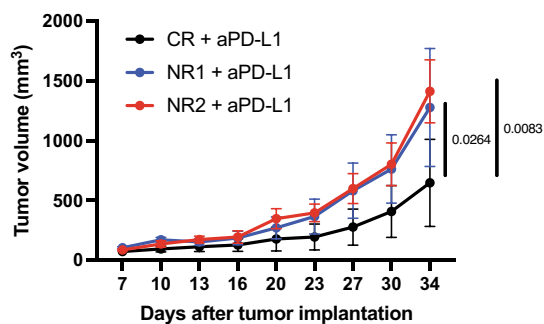
g



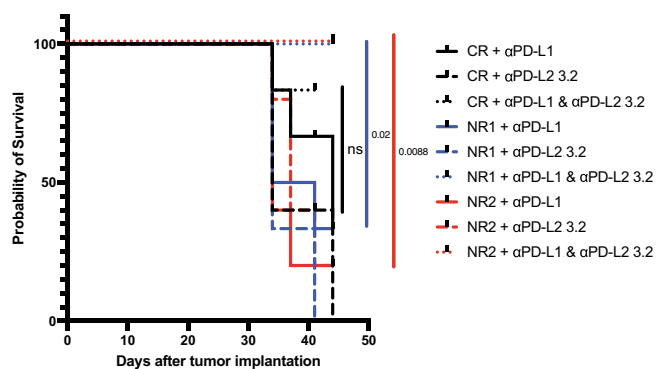
h



i



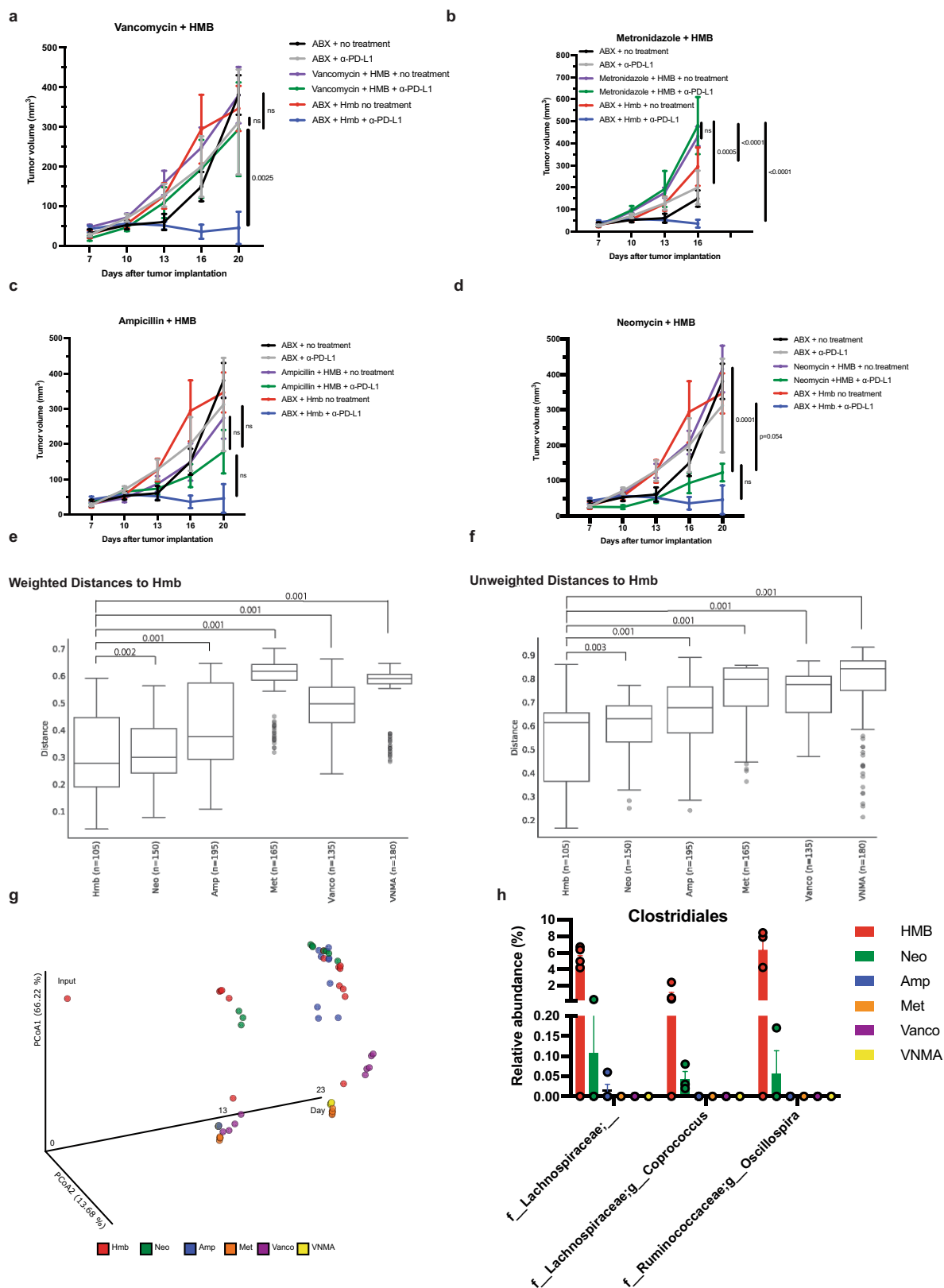
j



Extended Data Fig. 4 | See next page for caption.

Extended Data Fig. 4 | 16S sequencing of fecal samples, tumor growth, and survival of mice colonized with melanoma patient stool. (a) Patient characteristics for stool samples. *Samples were characterized as complete responder (CR) or non-responder (NR) based on RECIST 1.1 response criteria. Mean age is 56.3 years, mean BMI is 29.9 kg/m². **Stage at start of ICB treatment. (b–h) Bacterial community configuration and distances in fecal samples collected from three different sets of mice colonized with melanoma patient stool: complete responder (CR), Non-responder 1 (NR1) and Non-responder 2 (NR2) as well as input. (b) Principal coordinates analysis (PCoA) of unweighted UniFrac distance measurements based on the 16S sequencing analysis of the composition of bacterial communities at 7 day after gavage. Each coloured circle represented a fecal community sampled from a mouse belonging to the indicated donor group or input gavage sample. Pairwise unweighted UniFrac distances of the composition of bacterial communities in fecal samples within (c) CR and across NR1 and NR2 groups compared to CR (d) NR1 and across CR and NR2 groups compared to NR1 and (e) NR2 and across CR and NR1 groups compared to NR2. Pairwise weighted UniFrac distances of the composition of bacterial communities in fecal samples within (f) CR and across NR1 and NR2 groups compared to CR (g) NR1 and across CR and NR2 groups compared to

NR1 and (h) NR2 and across CR and NR1 groups compared to NR2. n= number of pairwise distances calculated between all samples in each group compared to the comparator group. *** q-values = 0.001, PERMANOVA. Minima, maxima, center, bounds, and percentiles of boxplots shown in source data. GF mice were colonized with stool from Responder (R) or Non-Responder (NR) melanoma patients treated with anti-PD-1, implanted with MC38 tumors, and given anti-PD-L1, anti-PD-L2 or anti-PD-L1 plus anti-PD-L2 mAbs. (i) Tumor growth in mice treated with anti-PD-L1 monotherapy. N = 6 mice for CR and NR1 groups and n = 5 mice for NR2 group. Significance determined by 2 way ANOVA and Tukey's multiple comparisons test and significant p values are indicated on graph. Error bars show standard error of the mean. (j) Survival of mice given anti-PD-L1, anti-PD-L2 or anti-PD-L1 plus anti-PD-L2 mAbs. Survival defined as number of live mice with tumors <2 cm³ or <50% ulcerated. N = 6 for CR + anti-PD-L1, CR+ anti-PD-L1 + anti-PD-L2, NR1 + anti-PD-L1, NR1 + anti-PD-L1 and anti-PD-L2, NR2 + anti-PD-L1 and anti-PD-L2, n = 5 for CR + anti-PD-L2, NR2 anti-PD-L1, NR2 anti-PD-L2, n = 3 for NR1 + anti-PD-L2. Significance of anti-PD-L1 monotherapy versus combination therapy for each group of mice shown and significance indicated on graph.

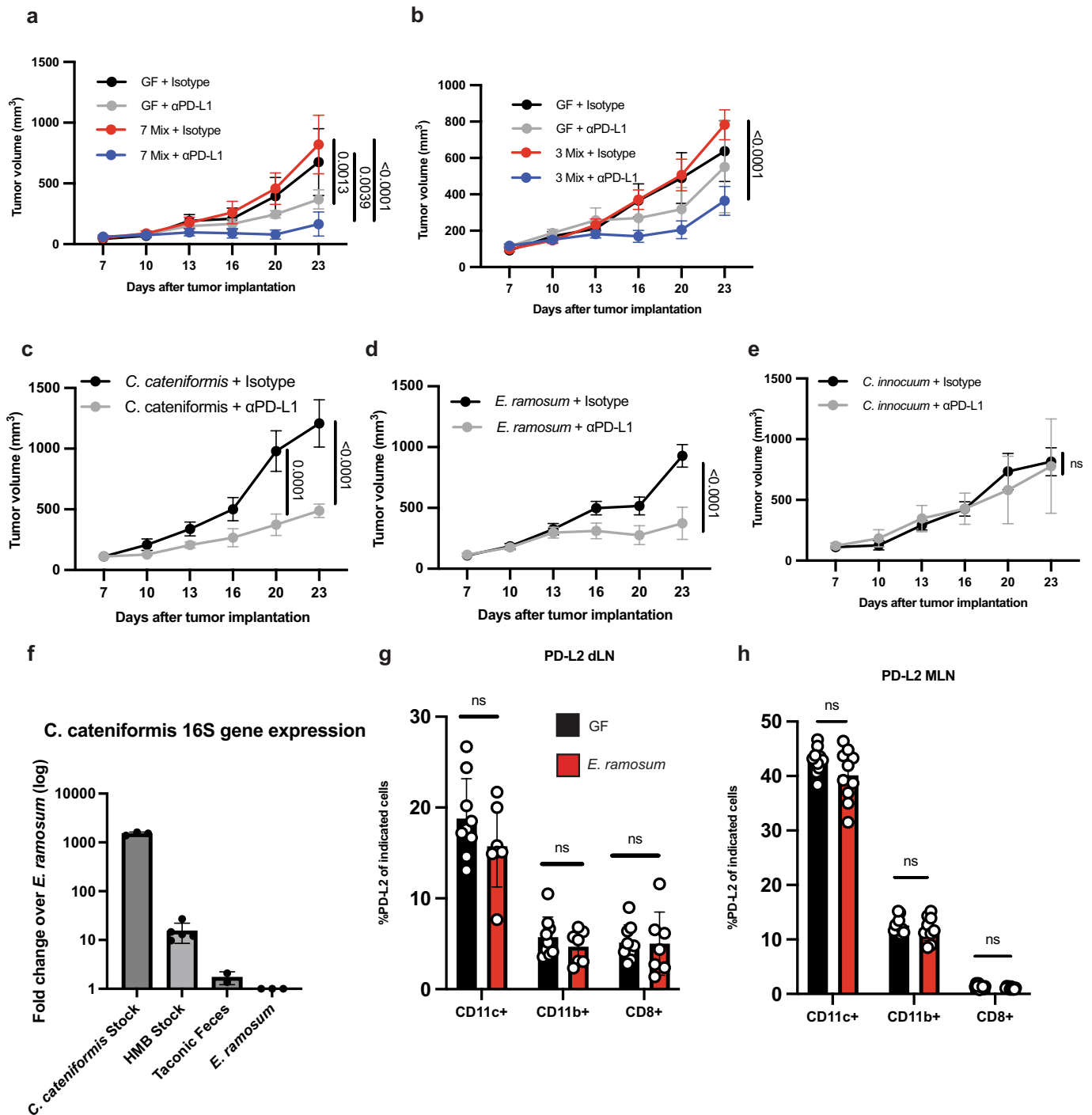


Extended Data Fig. 5 | See next page for caption.

Extended Data Fig. 5 | Individual antibiotic treatments and 16S sequencing show Gram-positive species are associated with an anti-tumor response.

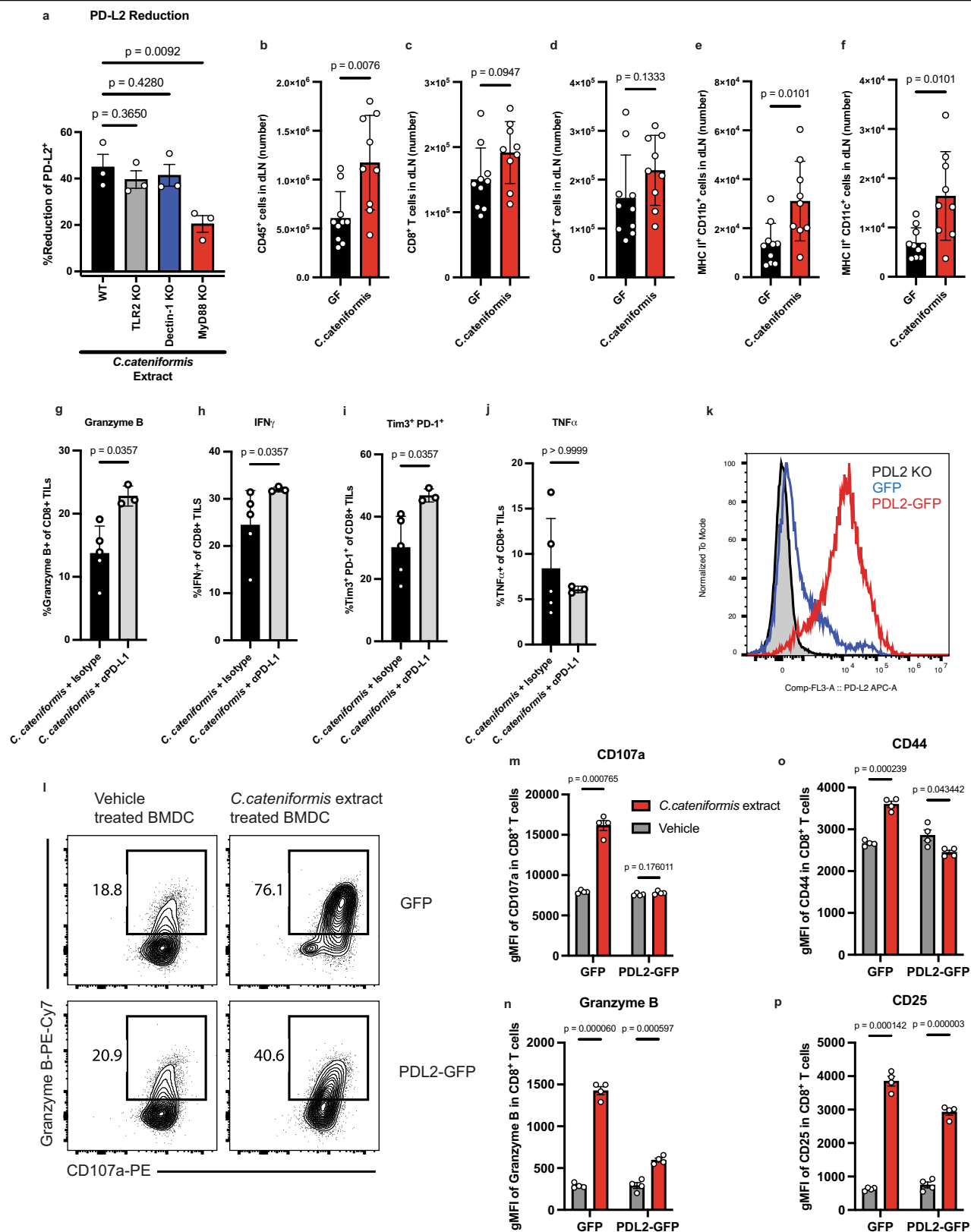
All mice were treated with Vancomycin, Neomycin, Metronidazole, and Ampicillin (VNMA) in the drinking water 4 days before tumor implantation until day 7 pi. VNMA mice continued with the antibiotic cocktail for the duration of the experiment. VNMA + HMB mice stopped VNMA at day 7 and were orally gavaged with HMB stock. Mice given individual antibiotics stopped VNMA at day 7 pi and water was replaced with an individual antibiotic and mice were orally gavaged with HMB stock. MC38 tumor growth curves in mice receiving HMB + (a) Vancomycin (Vanco) n = 5 mice per group (b) Metronidazole (Met) n = 5 mice per group (c) Ampicillin (AMP) n = 5 mice per group and (d) Neomycin (Neo) n = 5 mice for no treatment and n = 3 mice for anti-PD-L1 group with or without anti-PD-L1. N = 4 for VNMA groups and n = 5 for HMB groups. Significance determined by two-way ANOVA and Tukey's multiple comparisons test and significant p values between individual antibiotic treatments versus HMB or VNMA are shown. Error bars show mean and s.e.m. (e-f) Pairwise weighted and unweighted UniFrac distances of the composition of bacterial communities in fecal samples within HMB and across treatment groups compared to HMB. Each dot represented the weighted or unweighted UniFrac distance between

the configuration of bacterial populations as judged from the relative abundances of its members, determined by 16S sequencing, in fecal samples collected from members of the indicated treatment group. q-values were indicated for each group comparisons as determined by permutational analysis of variance (PERMANOVA) for beta diversity group significance. Minima, maxima, center, bounds, and percentiles of boxplots shown in source data. (g) Principal coordinates analysis (PCoA) of weighted UniFrac distance measurements based on the 16S sequencing data of the composition of bacterial communities in the fecal samples of mice with different treatment at day 13 and 23 pi. Each colored circle represented a fecal community sampled from a mouse belonging to the indicated antibiotic treatment group or input gavage sample. (h) The relative abundance of the taxa in the order of Clostridiales in each treatment group at day 23 pi after anti-PD-L1 treatment. These identified taxa were significantly (W-statistic = 39, 35 and 34 respectively, p-value < 0.05) associated with response to anti-PD-L1 by differential abundance testing of taxa between the responder group (HMB n = 5, Neomycin n = 3) to the non-responder group (ABX n = 3, Ampicillin n = 4, Vancomycin n = 3, and Metronidazole n = 2) using ANCOM (Analysis of Composition of Microbiomes).



Extended Data Fig. 6 | Narrowing down bacteria isolated from HMB stocks that promote anti-tumor immunity and suppress PD-L1. MC38 tumor growth in gnotobiotic mice colonized one week prior to tumor implantation with (a) Mix of overnight cultures of *Longicatenella caecimuris*, *Blautia hydrogenotrophica*, *Clostridium orbiscindens*, *Clostridium innocuum*, *Phocaeicola dorei*, *Coprobacillus cateniformis*, and *Erysipelatoclostridium ramosum* n = 4 mice for GF + Isotype, n = 5 mice per group for GF + anti-PD-L1, 7 mix + isotype, and 7 mix + anti-PD-L1 (b) mix of overnight cultures of *C. innocuum*, *C. cateniformis*, *E. ramosum* n = 4 mice for GF + isotype, n = 5 mice for GF + anti-PD-L1, n = 10 mice for 3 mix + Isotype, n = 9 mice for 3 mix + anti-PD-L1 (c) *C. cateniformis* n = 5 mice per group (d) *E. ramosum* n = 10 mice per group (e) *C. innocuum* n = 5 mice for isotype and n = 4 mice for anti-PD-L1. Significance at day 23 is shown and was determined by two-way ANOVA with Tukey's multiple comparisons test for a and b. Significance is shown and was measured by two-way ANOVA with Sidak's multiple comparisons test for all

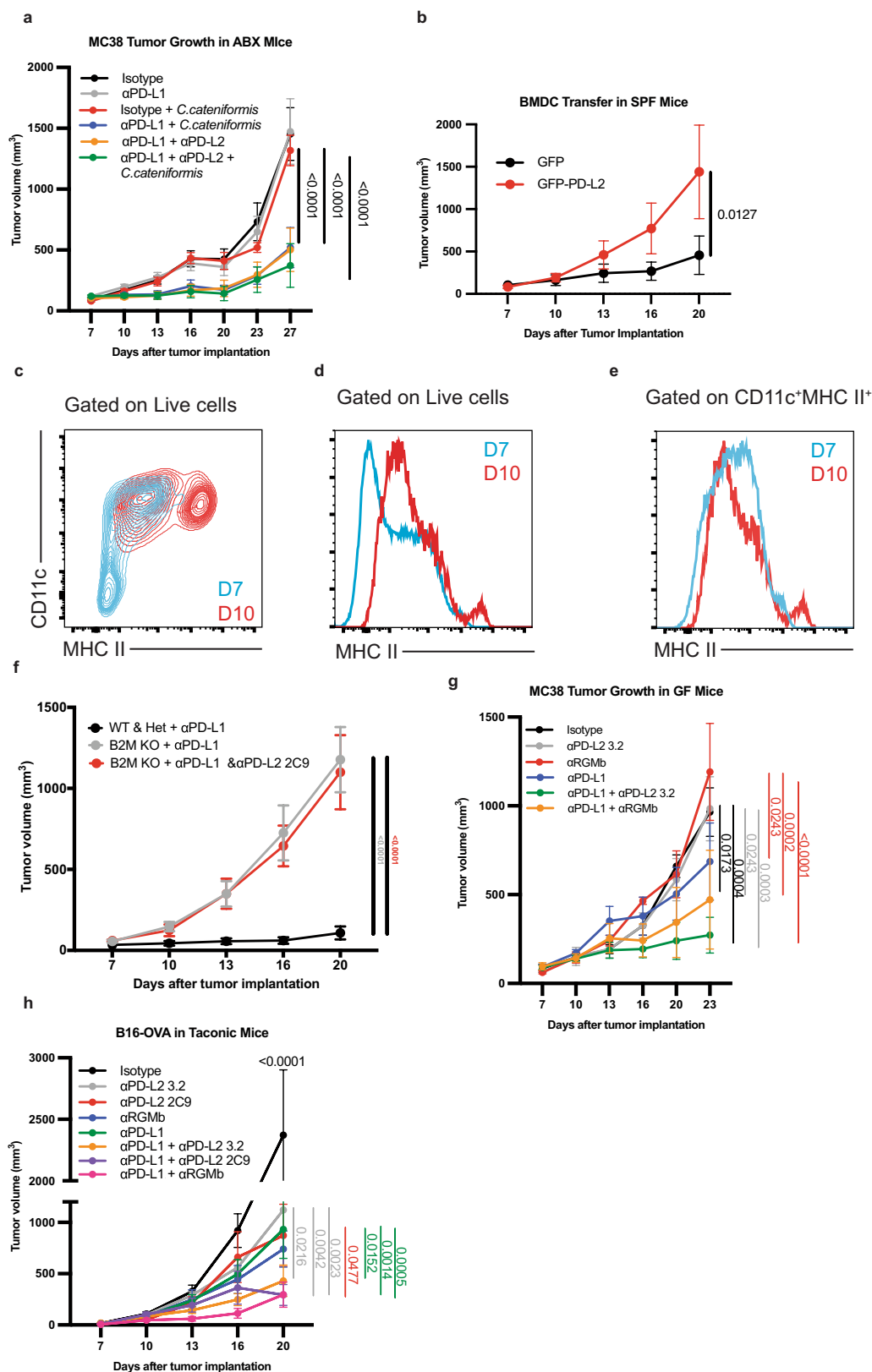
days was shown for c-e. Error bars for all tumor graphs show mean and s.e.m. (f) *C. cateniformis*-specific primers for the 16S gene were used to detect *C. cateniformis* in *C. cateniformis* stock, HMB stocks, Taonic feces, and *E. ramosum* stocks. *C. cateniformis* gene expression was normalized using the 16S universal primers in each group. N = 3 technical replicates for *C. cateniformis* and *E. ramosum* pure stocks, n = 5 biological replicates from 5 HMB stocks, n = 2 biological replicates of stool samples from two different Taonic mice. To show sequence specificity, data are shown as log fold change over the normalized *C. cateniformis*-specific 16S levels in *E. ramosum* stock. Error bars represent standard deviation. GF mice or GF mice monoclonized with *E. ramosum* one week prior to tumor implantation were sacrificed at day 10 p.i. PD-L2 was measured on MHCII+ CD11c+, MHCII+ CD11b+, and CD8⁺ T cells in (g) draining lymph nodes, n = 9 mice for GF and 7 mice for *E. ramosum* (h) MLN, n = 10 mice per group. Significance measured by Mann-Whitney test and error bars show mean and s.d.



Extended Data Fig. 7 | See next page for caption.

Extended Data Fig. 7 | *C. cateniformis* and its surface extracts impact immune function. (a) BMDCs from WT, TLR2 KO, Dectin-1 KO, and MyD88 KO mice were treated with surface extracts isolated from *C. cateniformis* pellets. PD-L2 expression was measured by flow cytometry. Percent reduction (compared to vehicle treatment) of PD-L2 expressing dendritic cells is shown. Significance measured by Kruskal-Wallis test and P values compared to WT are indicated on graph. Error bars show mean and s.d., n = 3 wells of BMDCs per group. (b–f) Isotype treated-GF versus GF mice monocolonized with *C. cateniformis* one week prior to tumor implantation were sacrificed at day 13 p.i. and dLNs were analyzed by flow cytometry. Frequencies of (b) CD45+ cells, (c) CD8+ T cells (d) CD4+ T cells (e) MHCII+ CD11b+ cells and (f) MHCII+CD11c+ cells. (b–f) n = 10 mice for GF and n = 9 mice for *C. cateniformis*, significance measured by unpaired, two-tailed Mann-Whitney test and P values are indicated on graphs, error bars show mean and s.d. (g–j) GF mice were monocolonized one week prior to tumor implantation and treated with either isotype or anti-PD-L1. Mice were sacrificed at day 18 p.i. and tumors were harvested for analysis. Frequencies of CD8+ T cells expressing (g) Granzyme B (h) IFN γ (i) TIM-3 and

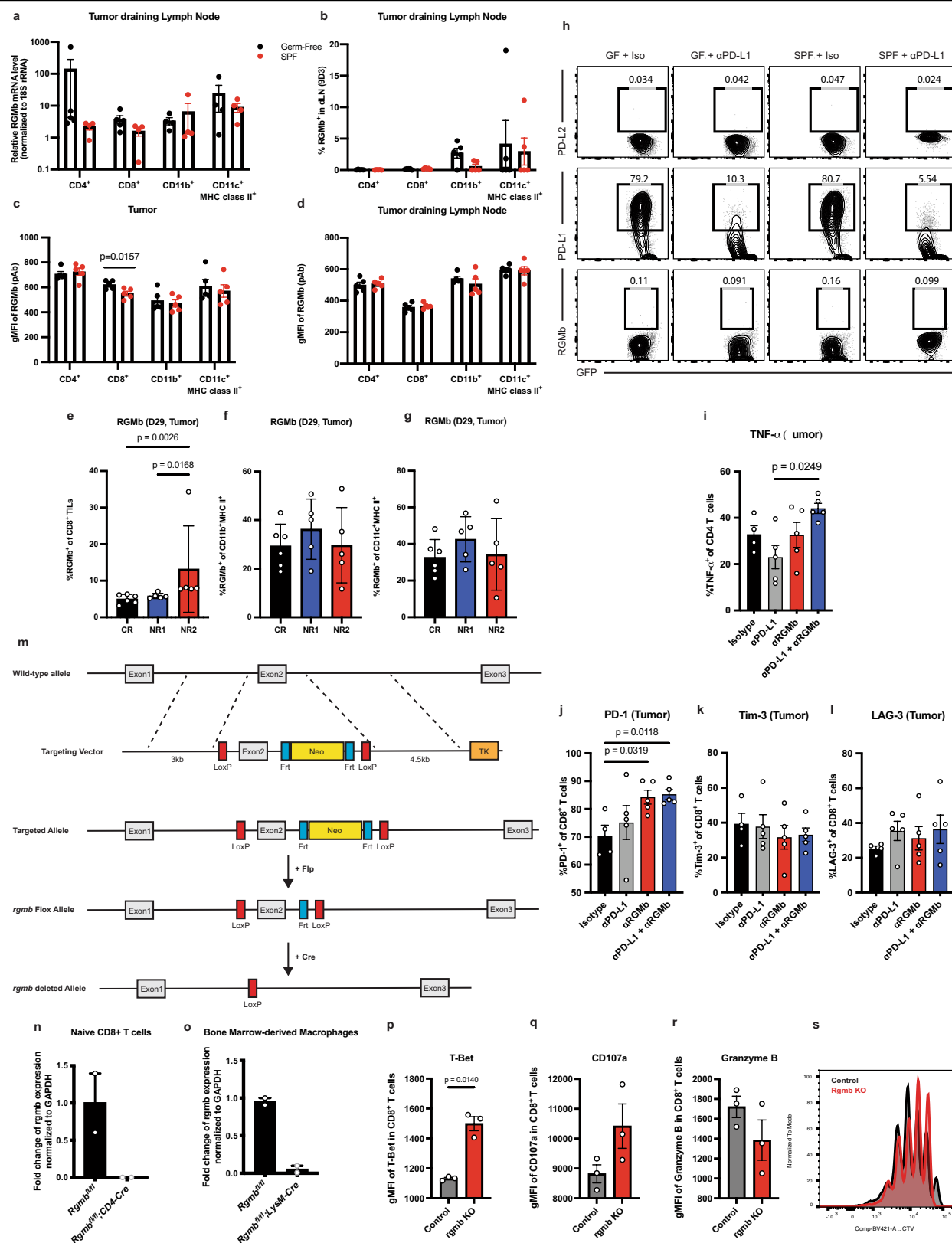
PD-1 and (j) TNF α . For (g–j) n = 5 mice for isotype and n = 3 mice for anti-PD-L1, significance determined by unpaired, two-tailed Mann-Whitney tests and P values are indicated on graphs, error bars show mean and s.d. (k) Histograms of PD-L2 expression on BMDCs measured by flow cytometry. Red = BMDCs transduced with PD-L2 GFP lentivirus, Blue = BMDCs transduced with control GFP lentivirus, Gray = BMDCs from PD-L2 KO mice. (l–p) BMDCs transduced with GFP lentivirus (GFP) or lentivirus expressing GFP and PD-L2 (PD-L2-GFP) were treated with *C. cateniformis* extract 24 h before co-culture with CD8+ T cells. Expression measured by flow cytometry. (l) Example of flow cytometry plots of Granzyme B and CD107a expression on CD8+ T cells. Quantification of mean fluorescence intensity of (m) CD107a and (n) Granzyme B expression on CD8+ T cells displayed in (l). Quantification of mean fluorescence intensity of (o) CD44 and (p) CD25 on CD8+ T cells. (m–p) Significance determined by unpaired, two-tailed t tests, with Welch correction and P values indicated on graph, n = 4 wells of BMDC- CD8+ T cell co-culture per group, error bars show mean and s.d.



Extended Data Fig. 8 | See next page for caption.

Extended Data Fig. 8 | *C. cateniformis* treatment and PD-L2 blockade impacts anti-tumor immunity. (a) Taconic mice were treated with broad spectrum antibiotics one week prior to tumor implantation. On days 7, 10, 13, 16 *C. cateniformis* or PBS was orally gavaged and antibodies were administered i.p. Significance between anti-PD-L1 + *C. cateniformis* treatment and the other groups at day 27 is shown. Significance measured by Two way ANOVA and Tukey's multiple comparisons test, n = 10 mice per group, error bars show mean and s.e.m. (b) B16-OVA tumor growth in SPF mice that received GFP or PD-L2-GFP BMDCs at tumor site 3 days after tumor implantation. Significance indicated on graph and measured by 2 way ANOVA and Sidak's multiple comparisons test, n = 10 mice per group, error bars show mean and s.e.m. (c-e) BMDCs were cultured for 7 (blue) or 10 (red) days and MHCII expression was measured by flow cytometry. (c) Expression of CD11c and MHCII gated on live cells from BMDC culture. (d) Histogram of MHCII expression gate on live cells from BMDC culture. (e) Histogram of MHCII expression gated on CD11c+ MHCII+ cells.

(f) Growth of MC38 tumor cells implanted subcutaneously in $\beta 2m^{-/-}$ mice (B2M KO), $\beta 2m^{+/-}$ (Het), and WT littermate controls. n = 5 mice per group for WT/het + anti-PD-L1 and B2M KO + anti-PD-L1 and n = 3 mice for B2M KO + anti-PD-L1 and anti-PD-L2. Significance indicated on graph measured by one-way ANOVA and Tukey's multiple comparisons, error bars show mean and s.e.m. Tumor growth of (g) MC38 tumor cells in GF mice treated with Isotype (n = 5 mice), anti-PD-L1 (n = 5 mice), anti-PD-L2 clone 3.2 (n = 5 mice), anti-RGMb (n = 4 mice), anti-PD-L1 + anti-PD-L2 3.2 (n = 4 mice), or anti-PD-L1 + anti-RGMb (n = 5 mice) and (h) B16-OVA tumor cells in Taconic mice treated with Isotype (n = 5 mice), anti-PD-L1 (n = 10 mice), anti-PD-L2 clone 3.2 (n = 5 mice), anti-PD-L2 clone 2C9 (n = 5 mice), anti-RGMb (n = 5 mice), anti-PD-L1 + anti-PD-L2 3.2 (n = 10 mice), anti-PD-L1 + anti-PD-L2 2C9 (n = 10 mice), or anti-PD-L1 + anti-RGMb (n = 10 mice). (g,h) Significance measured by Two-way ANOVA and Tukey's multiple comparisons, P values are shown on graph, error bars show mean and s.e.m.

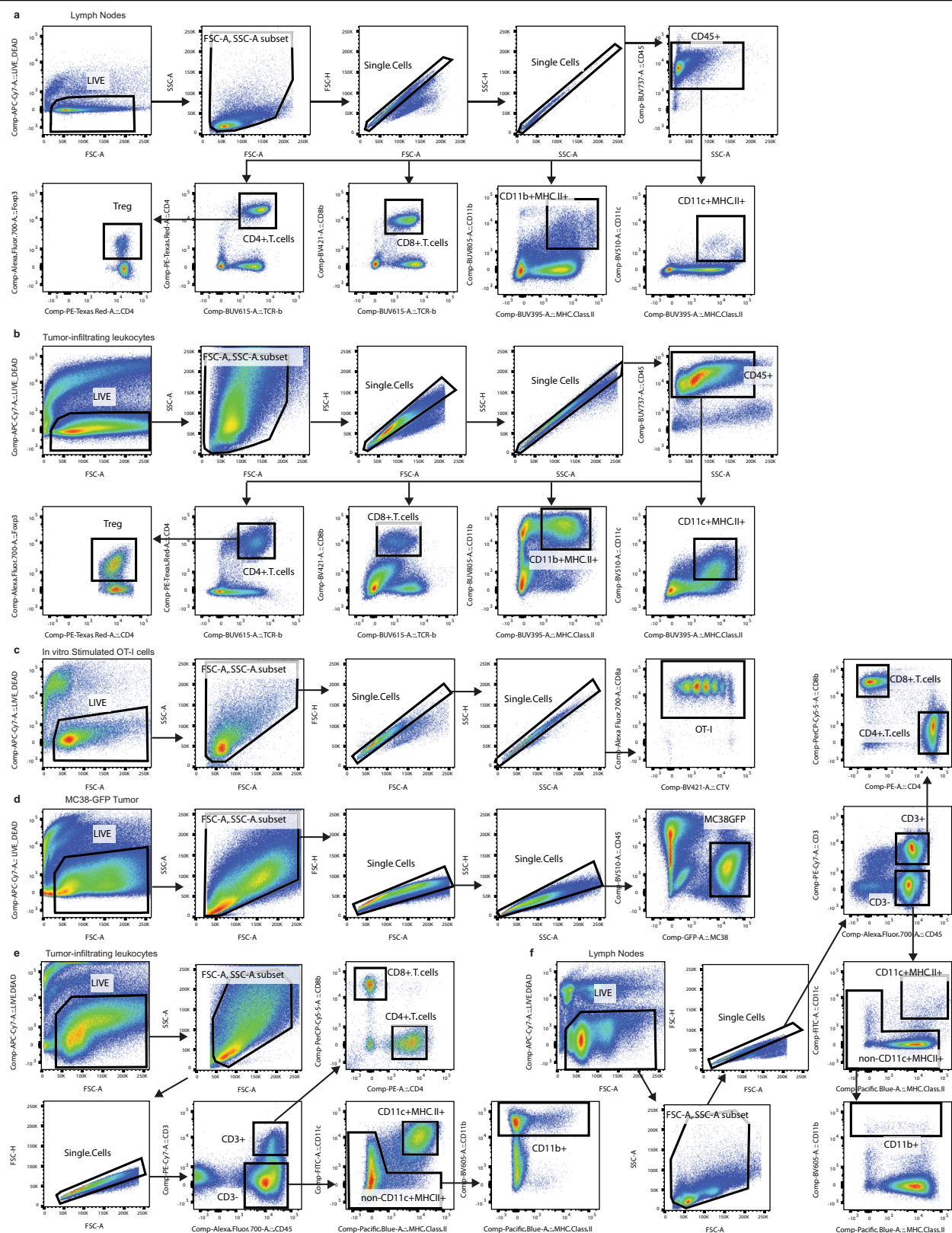


Extended Data Fig. 9 | See next page for caption.

Extended Data Fig. 9 | RGMb expression is modulated by the gut microbiota.

Tumor draining lymph nodes from GF and SPF mice implanted with MC38 tumor cells subcutaneously, as in Fig. 1a, were analyzed on day 11 after implantation. (a) Relative mRNA expression of RGMb in tumor draining lymph nodes of indicated cells. The levels of *rgmb* transcripts were normalized to expression of an internal control gene *18S rRNA*. N = 5 mice for GF and n = 4 mice for SPF and (b–d) cell surface expression of RGMb protein in CD4⁺ T cells, CD8⁺ T cells, CD11c⁺ MHCII⁺ and CD11b⁺ cells. (b) Frequencies of RGMb-expressing CD4⁺ T cells, CD8⁺ T cells, CD11c⁺ MHCII⁺ and CD11b⁺ cells were measured using 9D3 clone mAb in dLN, n = 5 mice per group. (c–d) Geometric Mean Fluorescent Intensity (gMFI) of RGMb was assessed in indicated populations from (c) tumor and (d) tumor draining lymph nodes using αRGMb polyclonal antibody, n = 5 mice per group. Significance measured by unpaired, two tailed Mann-Whitney test and significant p values indicated on graph, error bars show mean and s.d. (e–g) GF mice were colonized with stools from three patients who received anti-PD-1 therapy and responded or did not respond - Complete Responder (CR, n = 6) or Non-Responder 1 (NR1, n = 5) or Non-Responder 2 (NR2, n = 5). The mice were injected subcutaneously with MC38 tumor cells and treated with rat IgG2b isotype control. Frequencies of RGMb-expressing tumor-infiltrating (e) CD8⁺ T cells, (f) CD11b⁺ MHC II⁺ cells, and (g) CD11c⁺ MHC II⁺ cells were examined on post-implantation day 29. Significance measured by non-parametric one-way ANOVA with Dunn's multiple comparisons test and significant p values indicated on graph. Error bars show mean and s.d. (h) MC38 tumor cells expressing GFP were implanted in GF or SPF mice. The mice were treated with two doses of isotype control or anti-PD-L1 one week after tumor implantation, and tumors were harvested 13 days after tumor implantation. MC38-GFP cells were isolated and examined to measure PD-L2 (Upper), PD-L1 (Middle), and RGMb (Lower) expression by flow

cytometry. Representative of 5 mice per group. (i) GF mice were implanted with MC38 tumor cells subcutaneously and treated with indicated antibodies as in Fig. 1a. Tumor-infiltrating CD4⁺ T cells were isolated on day 11 after tumor implantation and stimulated with PMA/Ionomycin for 5 h. Frequencies of TNF-α producing cells among CD4⁺ T cell population were measured by intracellular staining and flow cytometry. N = 4 mice for isotype and n = 5 mice for anti-PD-L1, anti-RGMb, and anti-PD-L1 + anti-RGMb groups. Significance measured by non-parametric one-way ANOVA with Dunn's multiple comparisons and indicated on graph. Error bars show mean and s.d. (j–l) GF mice were implanted with MC38 tumor cells subcutaneously and treated with indicated antibodies as in Fig. 1a. Cells in tumor and tumor draining lymph node were analyzed on day 11 after tumor implantation. Frequencies of tumor infiltrating CD8⁺ T cells expressing (j) PD-1 (k) TIM-3 and (l) LAG-3. N = 4 mice for isotype and n = 5 mice for anti-PD-L1, anti-RGMb, anti-PD-L1 + anti-RGMb groups. Significance measured by non-parametric one-way ANOVA with Dunn's multiple comparisons and significant p values indicated on graphs. Error bars show mean and s.d. (m) Strategy to generate RGMb conditional knockout mice (n) Validation of CD4-Cre mediated deletion of RGMb in peripheral naïve CD8 T cells by qPCR (o) Validation of LysM-Cre mediated deletion of RGMb in bone marrow derived macrophages by qPCR, n = 2 mice per group. Error bars show mean and s.d. (p–s) WT or RGMb KO CD8⁺ T-cells were co-cultured with WT BMDCs. CD8⁺ T cells were analyzed by flow cytometry for (p) Mean Fluorescence Intensity (MFI) of T-Bet (q) MFI of CD107a (r) MFI of Granzyme B and (s) proliferation measured by Cell Trace Violet. N = 3 per group. Representative experiment of 3 experiments. Significance determined by unpaired Mann-Whitney test and significant p values indicated on graphs. Error bars show mean and s.d.



Extended Data Fig. 10 | Gating strategies for flow cytometric analysis. The following gating schemes were used to define CD11c⁺ MHC II⁺, CD11b⁺ MHC II⁺ cells, CD8⁺ T cells, CD4⁺ T cells and Treg cells in (a) draining lymph nodes and mesenteric lymph nodes and (b) tumor-infiltrating immune cells. (c) Gating strategy to examine OT-I cells stimulated by OVA-loaded BMDCs. (d) Gating

strategy used to analyze tumor cells from the mice implanted with MC38 tumor cells expressing GFP. Gating strategies used to sort CD4⁺ T cells, CD8⁺ T cells, CD11c⁺ MHC II⁺ cells and CD11b⁺ cells from (e) tumor-infiltrating leukocytes and (f) tumor draining lymph nodes.

Reporting Summary

Nature Portfolio wishes to improve the reproducibility of the work that we publish. This form provides structure for consistency and transparency in reporting. For further information on Nature Portfolio policies, see our [Editorial Policies](#) and the [Editorial Policy Checklist](#).

Statistics

For all statistical analyses, confirm that the following items are present in the figure legend, table legend, main text, or Methods section.

- | | |
|-------------------------------------|--|
| n/a | Confirmed |
| <input type="checkbox"/> | <input checked="" type="checkbox"/> The exact sample size (<i>n</i>), for each experimental group/condition, given as a discrete number and unit of measurement |
| <input type="checkbox"/> | <input checked="" type="checkbox"/> A statement on whether measurements were taken from distinct samples or whether the same sample was measured repeatedly |
| <input type="checkbox"/> | <input checked="" type="checkbox"/> The statistical test(s) used AND whether they are one- or two-sided.
<i>Only common tests should be described solely by name; describe more complex techniques in the Methods section.</i> |
| <input type="checkbox"/> | <input checked="" type="checkbox"/> A description of all covariates tested |
| <input type="checkbox"/> | <input checked="" type="checkbox"/> A description of any assumptions or corrections, such as tests of normality and adjustment for multiple comparisons |
| <input type="checkbox"/> | <input checked="" type="checkbox"/> A full description of the statistical parameters including central tendency (e.g. means) or other basic estimates (e.g. regression coefficient) AND variation (e.g. standard deviation) or associated estimates of uncertainty (e.g. confidence intervals) |
| <input type="checkbox"/> | <input checked="" type="checkbox"/> For null hypothesis testing, the test statistic (e.g. <i>F</i> , <i>t</i> , <i>r</i>) with confidence intervals, effect sizes, degrees of freedom and <i>P</i> value noted.
<i>Give <i>P</i> values as exact values whenever suitable.</i> |
| <input type="checkbox"/> | <input checked="" type="checkbox"/> For Bayesian analysis, information on the choice of priors and Markov chain Monte Carlo settings |
| <input type="checkbox"/> | <input checked="" type="checkbox"/> For hierarchical and complex designs, identification of the appropriate level for tests and full reporting of outcomes |
| <input checked="" type="checkbox"/> | <input type="checkbox"/> Estimates of effect sizes (e.g. Cohen's <i>d</i> , Pearson's <i>r</i>), indicating how they were calculated |

Our web collection on [statistics for biologists](#) contains articles on many of the points above.

Software and code

Policy information about [availability of computer code](#)

- | | |
|-----------------|---|
| Data collection | Raw 16S sequencing data was processed with QIIME2 pipelines and DADA2 was used for sequence, quality control, and feature table construction. BD FACS DIVA 9 software was used to collect data generated by BD TM LSR II, BD FACSymphony TM and BD FACS Aria TM II. qPCR data were collected using LightCycler 96 1.1 software. |
| Data analysis | Analysis of 16S data was performed using QIIME2, permutation of analysis variance (PERMANOVA), and Analysis of Composition of Microbiomes. All other statistical analyses were performed in Graphpad PRISM 9. FlowJo 10.8.1 software was used for flow cytometric analysis. |

For manuscripts utilizing custom algorithms or software that are central to the research but not yet described in published literature, software must be made available to editors and reviewers. We strongly encourage code deposition in a community repository (e.g. GitHub). See the Nature Portfolio [guidelines for submitting code & software](#) for further information.

Data

Policy information about [availability of data](#)

All manuscripts must include a [data availability statement](#). This statement should provide the following information, where applicable:

- Accession codes, unique identifiers, or web links for publicly available datasets
- A description of any restrictions on data availability
- For clinical datasets or third party data, please ensure that the statement adheres to our [policy](#)

16S sequencing data has been deposited to NIH. Bio Project number: PRJNA936792.

Field-specific reporting

Please select the one below that is the best fit for your research. If you are not sure, read the appropriate sections before making your selection.

☒ Life sciences ☐ Behavioural & social sciences ☐ Ecological, evolutionary & environmental sciences

For a reference copy of the document with all sections, see [nature.com/documents/nr-reporting-summary-flat.pdf](https://www.nature.com/documents/nr-reporting-summary-flat.pdf)

Life sciences study design

All studies must disclose on these points even when the disclosure is negative.

Sample size	Sample sizes were not predetermined and were indicated in the figure legends. 5-10 mice per group were chosen based on previous experience (DOI: 10.1038/s41590-019-0480-4) common practice in the field, and animal welfare guidelines and availability of animals, while minimizing the use of animals in accordance with animal care guidelines from the Harvard Medical School Standing Committee on Animals and the National Institutes of Health.
Data exclusions	Mice in which no tumor was visible 10 days after tumor implantation were excluded from the study
Replication	Experimental findings were repeated by multiple methods: repetitions of the exact experimental conditions, validation of findings using either blocking antibodies or knockout mice, confirming findings in multiple tumor models and in both Germ Free, antibiotic treated, and colonized mice. Number of replications indicate on figure legends and experiments were successfully replicated.
Randomization	All mice were treated identically until day 7 post implantation, at which point mice were randomly selected to be in isotype versus antibody treatment groups. Cell culture experiments were pooled before splitting into individual identical wells before being randomly assigned... vehicle versus C. cat extract groups.
Blinding	The investigators who colonized GF mice with patient stool and who took the tumor measurements for these mice were blinded until the completion of the experiment as to which patient stool was a responder versus non responder. Tumor growth curves were not plotted until all the data points collected. Experiments were performed blinded when possible. Blinding was not possible for many experiments as sterility of GF and ABX and purity of monocolonized mice had to be monitored throughout the experiment. To mitigate this, data were plotted and analyzed at the end of the experiment and measurements and analysis were performed by multiple people.

Reporting for specific materials, systems and methods

We require information from authors about some types of materials, experimental systems and methods used in many studies. Here, indicate whether each material, system or method listed is relevant to your study. If you are not sure if a list item applies to your research, read the appropriate section before selecting a response.

Materials & experimental systems	Methods
n/a Involved in the study	n/a Involved in the study
<input type="checkbox"/> <input checked="" type="checkbox"/> Antibodies	<input checked="" type="checkbox"/> <input type="checkbox"/> ChIP-seq
<input type="checkbox"/> <input checked="" type="checkbox"/> Eukaryotic cell lines	<input type="checkbox"/> <input checked="" type="checkbox"/> Flow cytometry
<input checked="" type="checkbox"/> <input type="checkbox"/> Palaeontology and archaeology	<input checked="" type="checkbox"/> <input type="checkbox"/> MRI-based neuroimaging
<input type="checkbox"/> <input checked="" type="checkbox"/> Animals and other organisms	
<input type="checkbox"/> <input checked="" type="checkbox"/> Human research participants	
<input checked="" type="checkbox"/> <input type="checkbox"/> Clinical data	
<input checked="" type="checkbox"/> <input type="checkbox"/> Dual use research of concern	

Antibodies

Antibodies used	anti-PD-L1 antibody (clone 10F.9G2), PD-1 antibody (clone RMP1-14), anti-PD-L2 antibody (clone 3.2), anti-PD-L2 antibody (clone GF17.2C9), anti-RGMb antibody (clone 307.9D1), recombinant anti-RGMb antibody (clone 307.9D1 Fv with either wild-type mouse IgG2a Fc or L234A/L235A/P329G (LALA-PG) triple mutant Fc effector silent antibody, rat IgG2b isotype control (LTF-2, BioXCell Cat# BE0090) or rat IgG2a isotype control (2A3 BioXCell Cat#BE0089), BUV395 anti-mouse CD8 clone H35-17.2 (BD Biosciences Cat#740278 1:200), Brilliant Violet 421 anti-mouse CD8 clone YTS156.7.7 (BioLegend Cat#126629 1:200), PerCP-Cy5.5 anti-mouse CD8 clone YTS156.7.7 (BioLegend Cat#126610 1:200), Alexa Fluor 700 anti-mouse CD8 clone 53-6.7 (BioLegend Cat#100730 1:200), BUV395 anti-mouse I-A/I-E clone 2G9 (BD Biosciences Cat#743876 1:500), Pacific Blue anti-mouse I-A/I-E clone M5/114.15.2 (BioLegend Cat#107620 1:500), BUV737 anti-mouse CD45.2 clone 104 (BD Biosciences Cat#564880 1:200), Brilliant Violet 711 anti-mouse CD44 clone IM7 (BioLegend Cat#103057 1:200), Brilliant Violet 605 anti-mouse CD44 clone IM7 (BioLegend Cat#103047 1:200), Alexa Fluor 700 anti-mouse CD45 clone 30-F11 (BioLegend Cat#103128 1:200), Brilliant Violet 510 anti-mouse CD45 clone 30-F11 (BioLegend Cat#103138 1:200), PE-Texas Red anti-mouse CD4 clone RM4-5 (ThermoFisher Scientific Cat#MCD0417 1:200), BUV564 anti-mouse CD4 clone GK1.5 (BD Biosciences Cat#612923 1:200), PE anti-mouse CD4 clone GK1.5 (BioLegend Cat#100408 1:200), PE-Cy7 anti-mouse IL-17A clone TC11-18H10.1 (BioLegend Cat#506922 1:200), Brilliant Violet 510 anti-mouse CD366 clone 5D12/TIM-3 (BD Biosciences Cat#747625 1:200), Brilliant Violet 711 anti-mouse CD366 clone 7D3 (BD Biosciences Cat#565566
-----------------	--

1:200), PE-CF594 anti-mouse CD11b clone M1/70 (BD Biosciences Cat#562317 1:200), BUV805 anti-mouse CD11b clone M1/70 (BD Biosciences Cat#741934 1:200), Brilliant Violet 605 anti-mouse CD11b clone M1/70 (BD Biosciences Cat#563015 1:200), BUV496 anti-mouse CD3 clone 145-2C11 (BD Biosciences Cat#564661 1:200), Brilliant Violet 570 anti-mouse CD3 clone 17A2 (BioLegend Cat#100225 1:200), PE-Cy7 anti-mouse CD3 clone 17A2 (BioLegend Cat#100220 1:200), Brilliant Violet 570 anti-mouse TCR clone H57-597 (BioLegend Cat#109231 1:200), BUV615 anti-mouse TCR clone H57-597 (BD Biosciences Cat#751212 1:200), APC anti-mouse IFN clone XMG1.2 (BioLegend Cat#505810 1:200), PerCP-eFluor 710 anti-mouse CD274 clone MH5 (Thermo Fisher Scientific Cat#46-5982-82 1:200), BUV737 anti-mouse CD80 clone 16-10A1 (BD Biosciences Cat#564670 1:200), PE-Cy7 anti-mouse CD11c clone HL3 (BD Biosciences Cat#558079 1:200), Brilliant Violet 510 anti-mouse CD11c clone HL3 (BD Biosciences Cat#562949 1:200), FITC anti-mouse CD11c clone N418 (BioLegend Cat#117306 1:200), PE anti-mouse CD11c clone N418 (BioLegend Cat#117307 1:200), PerCP-Cy5.5 anti-mouse TNF clone MP6-XT22 (BioLegend Cat#506322 1:200), Brilliant Violet 711 anti-mouse TNF clone MP6-XT22 (BioLegend Cat#506349 1:200), FITC anti-human/mouse Granzyme B clone GB11 (BioLegend Cat#515403 1:200), PE-Cy7 anti-human/mouse Granzyme B clone QA16A02 (BioLegend Cat#372214 1:200), Brilliant Violet 605 anti-mouse CD279 clone 29F.1A12 (BioLegend Cat#135220 1:200), PE-Cy7 anti-mouse Galectin-9 clone RG9-35 (BioLegend Cat#136113 1:200), Brilliant Violet 510 anti-mouse CD40 clone 3/23 (BD Biosciences Cat#745041 1:200), PerCP-Cy5.5 anti-human/mouse/rat CD278 clone C398.4A (BioLegend Cat#313518 1:200), PE-Cy7 anti-mouse CD252 clone RM134L (BioLegend Cat#108813 1:200), Biotinylated anti-mouse RGMb polyclonal antibody (R&D Systems Cat#BAF3597 1:200), APC streptavidin (BioLegend Cat#405243 1:200), Brilliant Violet 605 anti-mouse CD86 clone GL1 (BD Biosciences Cat#563055 1:200), PE anti-mouse CD275 (BioLegend Cat#107405 1:200), Brilliant Violet 421 anti-mouse CD273 clone TY25 (BioLegend Cat#107219 1:200), APC anti-mouse CD273 clone TY25 (BioLegend Cat#107210 1:200), PE anti-mouse CD223 clone eBioC9B7W (Thermo Fisher Scientific Cat#12-2231-82 1:200), PE-Cy7 T-bet clone 4B10 (BioLegend Cat#644823 1:200), PE anti-mouse CD107a clone 1D4B (BioLegend Cat#121612 1:200), BV711 anti-mouse IL-2 clone JES6-5H4 (BioLegend Cat#503837 1:200). Alexa Fluor 594 anti-RGMb clone 9D3 antibody (1:100) was generated in Gordon Freeman's laboratory as previously described in Y. Xiao, S. Yu, B. Zhu, D. Bedoret, X. Bu, L. M. Francisco, P. Hua, J. S. Duke-Cohan, D. T. Umetsu, A. H. Sharpe, R. H. DeKruyff, G. J. Freeman, RGMb is a novel binding partner for PD-L2 and its engagement with PD-L2 promotes respiratory tolerance. J Exp Med. 211, 943–959 (2014)

Validation

All commercially available antibodies were verified according to the manufacturer's specifications. RGMb 9D1, RGMb 9D3, and PD-L2 3.2 and 2C9 were provided by Gordon Freeman and validated for selective binding to mouse and human RGMb, flow cytometric assay and in vivo applications in previous publication (Y. Xiao, S. Yu, B. Zhu, D. Bedoret, X. Bu, L. M. Francisco, P. Hua, J. S. Duke-Cohan, D. T. Umetsu, A. H. Sharpe, R. H. DeKruyff, G. J. Freeman, RGMb is a novel binding partner for PD-L2 and its engagement with PD-L2 promotes respiratory tolerance. J Exp Med. 211, 943–959 (2014)). anti-RGMb triple mutant Fc effector silent antibody was generated by Gordon Freeman and validated using the same specifications as in Y. Xiao, S. Yu, B. Zhu, D. Bedoret, X. Bu, L. M. Francisco, P. Hua, J. S. Duke-Cohan, D. T. Umetsu, A. H. Sharpe, R. H. DeKruyff, G. J. Freeman, RGMb is a novel binding partner for PD-L2 and its engagement with PD-L2 promotes respiratory tolerance. J Exp Med. 211, 943–959 (2014)

Eukaryotic cell lines

Policy information about cell lines

Cell line source(s)

MC38 were gifted from D. Vignali University of Pittsburgh School of Medicine, B16.F10 were gifted from G. Dranoff (Novartis Institutes for Biomedical Research) and modified to express OVA. E0771 (ATCC Cat#CRL3461), LLC (ATCC Cat#CRL1642) and MB49 (Sigma Cat#SCC148) were purchased from manufacturers and PY8119 (ATCC Cat#CRL3278) was purchased and modified to express OVA. Gibco Viral Production cells (A derivative of HEK 293F cell line) were purchased from ThermoFisher Scientific (Cat#A35827).

Authentication

Cell lines were verified by the manufacturer's websites and regularly checked by morphology. MC38 and B16.F10 were validated through whole exome sequencing. B16-OVA cells were validated based on selection in puromycin. MC38-GFP were validated by flow cytometry based on expression of the selectable marker GFP

Mycoplasma contamination

Cell lines were tested for mycoplasma by PCR and confirmed mycoplasma negative.

Commonly misidentified lines
(See ICLAC register)

E0771 is also listed as E0771 or EO 771.

Animals and other organisms

Policy information about studies involving animals; ARRIVE guidelines recommended for reporting animal research

Laboratory animals

The animal facility was operated by Harvard Center for Comparative Medicine with the following housing conditions: 12:12 Light-Dark cycle, room temperature between 68–79°F, humidity level 40–65%. 6-week old C57BL/6 female mice were purchased from Taconic Biosciences. B2m-deficient mice were obtained from The Jackson Laboratory. 6–10 weeks old female B2m-deficient mice were used for experiments. Germ-free mice were maintained in the germ-free facility at Harvard Medical School. All experimental mice were housed in specific pathogen-free conditions or germ-free isolators. RGMb conditional knockout mice were generated by homologous integration of a construct, which contains LoxP sites flanking exon 2 of rgmb gene and Neomycin cassette (Extended Data Fig. 9m). Neo flanked by Frt sites were removed by breeding mice with germ-line transmission of the homologously integrated construct and a Flp delete strain. RGMb conditional knockout mice were further crossed with LysM-Cre (Jackson Laboratory, #004781) or CD4-Cre mice (Jackson Laboratory, #022071), to generate Macrophage-specific or T-cell specific conditional knockout mice, respectively. 6–10 weeks old female Rgmb conditional knockout mice were used for experiments.

Wild animals

No wild animals were used in the study

Field-collected samples

No field-collected samples were used in the study

Ethics oversight

All mice were used in accordance with animal care guidelines from Harvard Medical School Standing Committee on Animals and the National Institutes of Health.

Note that full information on the approval of the study protocol must also be provided in the manuscript.

Human research participants

Policy information about [studies involving human research participants](#)

Population characteristics

For in vivo studies involving human samples, stool samples were obtained from melanoma patients treated with immune checkpoint blockade (ICB; anti-PD-1). Fresh frozen fecal samples were used, including one responder (CR, Sample ID 274(14)) and two non-responders (NR1, sample ID 376 (unpublished) and NR2 Sample ID 426(14)). Patients were selected based on their tumor progression and overall survival after surgery and subsequent treatment with PD-1 blockade (pembrolizumab or nivolumab). Response to treatment was assessed with radiographic imaging and according to Response Evaluation Criteria in Solid Tumors (RECIST 1.1)(31); patients with complete or partial response or stable disease ≥ 6 months were classified as responders and those with stable disease < 6 months or progressive disease were classified as non-responders. The mean patient age was 56.3 years (50-62), and mean BMI was 29.9 kg/m² (20.4-42.31). The complete responder sample was taken 2 years post-treatment. Complete response was identified 3 years prior to fecal sample collection. The non-responder samples were taken during treatment, 3 months to 1 year after the start of ICB.

Recruitment

Fecal samples only from patients with melanoma treated with anti-PD-1 therapy were used in this study. Melanoma patients treated at MD Anderson Cancer Center were recruited as per IRB protocols 2012-0846 and PA15-0232.

Ethics oversight

Samples were collected under approved IRB protocols 2012-0846 and PA15-0232.

Note that full information on the approval of the study protocol must also be provided in the manuscript.

Flow Cytometry

Plots

Confirm that:

- ☒ The axis labels state the marker and fluorochrome used (e.g. CD4-FITC).
- ☒ The axis scales are clearly visible. Include numbers along axes only for bottom left plot of group (a 'group' is an analysis of identical markers).
- ☒ All plots are contour plots with outliers or pseudocolor plots.
- ☒ A numerical value for number of cells or percentage (with statistics) is provided.

Methodology

Sample preparation

Tumors were harvested on post-implantation days 10-16, mechanically dissociated, and incubated in DPBS containing calcium, magnesium and 250 units/mL of Type 1 Collagenase (Worthington Biochemical Corporation) for 20 minutes at 37 °C with gentle rocking. After filtration, tumor-infiltrating lymphocytes were isolated by Percoll density gradient (40%/70%) centrifugation at 800xg for 20 minutes without brake. The interface of the Percoll layers were recovered for further analyses. Primary mouse cells were isolated from draining lymph node and mesenteric lymph nodes and tumors. Single cell suspensions were prepared with a 70µm cell strainer. Cells were incubated with TruStain FcX (BioLegend Cat#101319) to block Fc receptors prior to staining. Cells were stained with LIVE/DEAD TM Fixable Near-IR Dead Cell Stain Kit (Thermo Fisher Scientific Cat#L34975) according to the manufacturer's instructions. Surface antigen staining was performed in DPBS containing 1% FBS and 2 mM EDTA, followed by intracellular staining using the eBioscience TM FoxP3/Transcription Factor Staining Buffer Set (Thermo Fisher Scientific Cat#00-5523-00). For intracellular cytokine staining, isolated cells were stimulated with 50 ng/mL of Phorbol 12-myristate 13-acetate and 500 ng/mL of ionomycin for 5 hours in the presence of 1X GolgiPlug protein transport inhibitor (BD Biosciences Cat#555029) and 1X GolgiStop protein transport inhibitor (BD Biosciences Cat#554724) prior to intracellular staining.

Instrument

Flow cytometry analyses were performed on a BD TM LSR II or BD FACSymphony TM. For cell sorting, a BD FACSAria TM II was used.

Software

Data were analyzed using FlowJo software 10.8.1

Cell population abundance

Samples were sorted directly into RLT buffer and used for data analysis

Gating strategy

Cells were identified using FSC/SSC gate followed by FSC-W/FSC-H to gate for single cells followed by SSC-W/SSC-H for single cells. Live CD45+ cells were selected using CD45+ LIVE/DEAD- gate. MCHII+ CD11b+ or MCHII+ CD11c+ cells were selected and PD-L2 expression was measured. For T cell analysis after selection of CD45+LIVE cells, TCRb+ CD4+ or TCRb+CD8 cells were selected and RGMb+ cell were analyzed.

- ☒ Tick this box to confirm that a figure exemplifying the gating strategy is provided in the Supplementary Information.